

JGR Atmospheres



RESEARCH ARTICLE

10.1029/2024JD043015

Key Points:

- Eight months of continuous measurements of methane mole fraction and stable isotopes (δ¹³C, δ²H) in an Eastern European urban environment
- Source mix was dominated by fossil emissions (57%), plus biogenic emissions (38%) in summer and pyrogenic sources in winter (5%)
- Atmospheric Lagrangian particle dispersion model and used emission inventory lack spatial resolution to successfully reproduce observations

Supporting Information:

Supporting Information may be found in the online version of this article.

Correspondence to:

J. van Es, j.d.vanes@uu.nl

Citation:

van Es, J., van der Veen, C., Baciu, C., Hmoudah, M., Menoud, M., Henne, S., & Röckmann, T. (2025). Methane sources in Cluj-Napoca, Romania: Insights from isotopic analysis. *Journal of Geophysical Research: Atmospheres*, *130*, e2024JD043015. https://doi.org/10.1029/2024JD043015

Received 22 NOV 2024 Accepted 2 AUG 2025

Author Contributions:

Thomas Röckmann

Data curation: Jacoline van Es,
Stephan Henne
Formal analysis: Jacoline van Es
Funding acquisition: Thomas Röckmann
Investigation: Jacoline van Es
Methodology: Carina van der Veen,
Calin Baciu, Thomas Röckmann
Resources: Carina van der Veen,
Calin Baciu, Mustafa Hmoudah
Software: Jacoline van Es,
Malika Menoud
Supervision: Thomas Röckmann

Conceptualization: Jacoline van Es.

© 2025 The Author(s).

This is an open access article under the terms of the Creative Commons

Attribution-NonCommercial License, which permits use, distribution and reproduction in any medium, provided the original work is properly cited and is not used for commercial purposes.

Methane Sources in Cluj-Napoca, Romania: Insights From Isotopic Analysis

Jacoline van Es¹, Carina van der Veen¹, Calin Baciu², Mustafa Hmoudah², Malika Menoud¹, Stephan Henne³, and Thomas Röckmann¹

¹Institute for Marine and Atmospheric Research Utrecht (IMAU), Utrecht University, Utrecht, The Netherlands, ²Faculty of Environmental Science and Engineering, Babeş-Bolyai University, Cluj-Napoca, Romania, ³Swiss Federal Laboratories for Materials Science and Technology (Empa), Dübendorf, Switzerland

Abstract Increased emissions of methane (CH₄) have contributed 0.3–0.8°C to global temperature rise since preindustrial times. Reducing these emissions is crucial to mitigate climate change. Measurements of the isotopic composition of CH₄ (δ^{13} C and δ^{2} H) can be used to distinguish various sources of CH₄. This study reports continuous measurements of CH₄, δ^{13} C and δ^{2} H for 8 months in Cluj-Napoca, Romania. An automated extraction and a purification system, coupled to an isotope ratio mass spectrometer alternately measured δ^{13} C and δ^2 H of CH₄ with 20-min time resolution at the campus of the Babes-Bolyai University. In addition, point source samples were measured to isotopically characterize CH₄ sources in the region. The time series show regular CH₄ elevations during the night, occasionally superimposed on multiday events. From these elevations, we identified three main CH₄ emission categories: Transylvanian biogenic gas (75%); biogenic emissions from rivers and wastewater (38%), predominantly observed during the summer; and a third source emitting ¹³Cenriched CH₄ in winter, likely of pyrogenic origin (5%). We simulated the CH₄ mole fraction at the measurement site using Lagrangian footprints generated from the FLEXPART-COSMO model convolved with emissions from the TNO-CoCO2 inventory. The simulations show that the emission inventory is not granular enough to represent the city center. The strong underestimation in winter suggests that the emission inventory did not include the pyrogenic winter source. When the model accurately estimated the CH₄ mole fraction, it also predicted the isotopic compositions well.

Plain Language Summary Methane is a strong greenhouse gas, and its emissions need to be strongly reduced to limit global warming. We need to know which types of sources are most important in different parts of the world to develop efficient emission mitigation strategies. We present 8 months of measurements of the isotopic composition of methane and use these data to characterize the source mix of methane in the city of Cluj-Napoca, Romania. Emissions from the natural gas distribution network and from biological processes are the most important source categories in this area.

1. Introduction

Reducing greenhouse gas (GHG) emissions is the main objective for policies aimed at mitigating climate change. In the 2015 Paris Agreement on climate change, countries agreed to limit global warming to 2° C compared to preindustrial levels and take efforts to limit it to 1.5° C. The increase of methane (CH₄) in the atmosphere threatens this goal (Nisbet et al., 2023). Therefore, 159 countries joined the Global Methane Pledge and committed to reduce methane emissions by at least 30% in 2030 compared to 2020 (IEA, 2023). The global methane mole fraction increased from about 700 parts per billion (ppb) in the preindustrial period to 1923 ppb in 2022 (Lan et al., 2022; MacFarling Meure et al., 2006). Particularly strong growth rates of more than 15 ppb/year occurred from 2020 till 2023 (Nisbet et al., 2023; Saunois et al., 2020). CH₄ is a strong greenhouse gas with a global warming potential that is 86 times higher than CO₂ over a short (20-year) timescale. Accordingly, anthropogenic CH₄ emissions have increased global temperature by 0.3– 0.8° C since pre-industrial times (Calvin et al., 2023). CH₄ has a shorter lifetime in the atmosphere then CO₂ of 9.1 ± 0.9 years and an inter-hemispheric mixing time of 1 year, making it well mixed in the atmosphere. Therefore, reducing CH₄ emissions can lead to a decrease in its atmospheric mole fraction on a relatively short timescale, making CH₄ emission reduction relevant for climate mitigation policies (Nzotungicimpaye et al., 2023; Ocko et al., 2021).

CH₄ is produced both naturally and anthropogenically via several pathways, which are often categorized as microbial, thermogenic, and pyrogenic (Calvin et al., 2023). Numerous measurement and model approaches are

VAN ES ET AL. 1 of 21



Journal of Geophysical Research: Atmospheres

10.1029/2024JD043015

Validation: Stephan Henne
Visualization: Jacoline van Es
Writing – original draft: Jacoline van Es
Writing – review & editing:
Thomas Röckmann

used to quantify CH_4 emissions for different regions around the globe (Chandra et al., 2024; Townsend-Small et al., 2012; Zavala-Araiza et al., 2018). These data have revealed large emissions in most regions of the world. The CH_4 mole fraction measurements are evaluated with models of various complexities, from simple mass balance models to inverse models (Bergamaschi et al., 2022; Henne et al., 2016; Petrescu et al., 2021; Ramsden et al., 2022; Saunois et al., 2020).

These investigations have been synthesized to produce a global methane budget, estimating the contribution of the CH₄ sources and sinks (Saunois et al., 2020). The main anthropogenic emissions are from natural gas, agriculture and waste, and biomass burning and biofuel burning (Saunois et al., 2020). The anthropogenic CH₄ emissions have been steadily increasing over the past century due to increased demand for livestock and energy.

Local emissions can be quantified via various approaches. One approach is mobile ground-based surveys that reveal emissions from, for example, the gas network (Balcombe et al., 2017; Defratyka et al., 2021; Maazallahi et al., 2020; Weller et al., 2020) and wastewater (Fernandez et al., 2022). Other methods are airborne observations with drones and aircraft (Andersen et al., 2023; Fiehn et al., 2023; Hollenbeck et al., 2021; Lavoie et al., 2015), and ground- and space-based total column observations (Dowd et al., 2024; Liu et al., 2024; Plant et al., 2022).

Because different CH_4 sources are often colocated and CH_4 is well mixed for a top-down atmospheric monitoring study, it is impossible to distinguish the CH_4 sources with CH_4 mole fraction measurements alone. Fortunately, the main CH_4 production pathways produce CH_4 with different isotopic compositions, enabling identification of the production pathway via the stable isotopic composition of CH_4 and thereby, to some extent, the source. The isotopic values for the mentioned processes have been synthesized and presented in Sherwood et al. (2021) with additions in Menoud et al. (2022a, 2022b) and Townsend-Small et al. (2016). Knowing the isotopic source signature might seem obsolete when samples are taken near a known source; however, its significance arises when a source is unknown or when CH_4 from various sources is mixed. This source mixing typically occurs at locations where several sources emit CH_4 in close proximity, for example, in urban environments (Menoud et al., 2021). The CH_4 isotopic measurements also improve inverse estimations of CH_4 by enabling better source differentiation (Basu et al., 2022; Thanwerdas et al., 2024).

Most isotope measurements are carried out in a laboratory on samples that were collected in the field (Beck et al., 2012; Fernandez et al., 2022; Fiehn et al., 2023; Lu et al., 2021; Maazallahi et al., 2020). In addition to this, field deployable analytical systems to measure CH₄ isotopes have become available (Eyer et al., 2016; Röckmann et al., 2016). Both infield and sample measurements use either optical isotope ratio spectroscopy (OIRS) or isotope ratio mass spectrometry (IRMS) (Hoheisel & Schmidt, 2023; Menoud, Van Der Veen, Maazallahi, et al., 2022; Röckmann et al., 2016). The continuous isotope measurements provide insight into prominent sources near the sampling location. For example, two campaigns conducted in the Netherlands (Cabauw and Lutjewad) detected mainly agricultural sources, despite Lutjewad being close to a gas extraction site (Menoud et al., 2020; Röckmann et al., 2016). A study in Krakow, Poland, indicated emissions primarily from coal mining (Menoud et al., 2021). For this study, we employed an identical IRMS setup as Menoud et al. (2021) to measure the CH₄ mole fraction, δ^{13} C and δ^{2} H in the urban environment of Cluj-Napoca, Romania. Analysis of the meteorological situation and model simulations serve to support data interpretation. Previous studies have primarily focused on Western Europe, and those conducted in Eastern Europe were limited to short time frames, such as daytime or summer periods. Therefore, investigating CH₄ emissions in an Eastern European city helps close this data gap.

Cities are responsible for 70% of GHG emissions, with the city center being a major hotspot for CH_4 emissions (Hopkins et al., 2016). This makes cities very important for mitigating climate change. Municipalities can implement local policies effectively without having to go through many administrative layers (Hemati et al., 2024; Hopkins et al., 2016). In 2018, 55% of the world population lived in cities, with the projection of 68% in 2050 (United Nations, 2019); therefore, mitigating climate change in cities will become even more important than before. Previous studies have been performed in cities around the globe. These showed that emissions varied between cities, for example, gas leaks dominating in Utrecht (Maazallahi et al., 2020), emissions from wastewater in Bucharest (Fernandez et al., 2022), and both sources in Paris (Defratyka et al., 2021). Additionally, in Hamburg, a mixture of emissions from the river (microbial) and fossil fuel sources has been found (Forstmaier et al., 2023; Maazallahi et al., 2020).

VAN ES ET AL. 2 of 21

inelibrary.wiley.com/doi/10.1029/2024JD043015 by Physikalisch Tec Bundesanstalt, Wiley Online Library on [27/11/2025]. See the Term

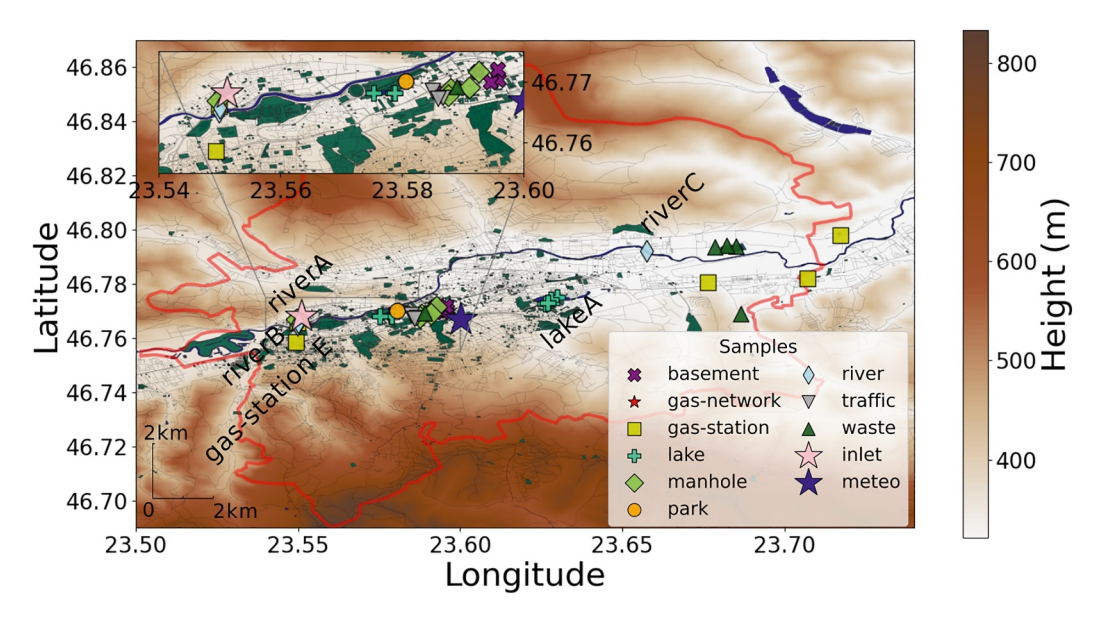


Figure 1. Orographic map of Cluj-Napoca and the surrounding area. The red star is the measurement site, the blue star is the meteorological measurement station, and the dots are sampling locations, colored by the source categories. The river is colored blue and the wetlands green. The names in the map are locations referred to in the results. This map is 18 km wide by 20 km high. The subset covers 2.5 km by 1.3 km. Note: most gas-network samples were taken from the gas network in the university building and are therefore not visible on the map.

In this study, the measurements are compared to simulations with an atmospheric model. This comparison can reveal inconsistencies in emission inventories or model assumptions, helping to identify over- or underestimated sources.

2. Materials and Methods

2.1. Measurement Site

Continuous measurements of the CH_4 mole fraction and isotopic composition were conducted in Cluj-Napoca (46° 46′N, 23° 37′E), located in the Cluj region in Romania (Figure 1). To the north and south are the Vârful Lomb Hill and Vârful Peană Hill, respectively. In the valley flows the Canalul Someşul Mic River from west to east, providing water to lakes and wetlands that support the production of microbial CH_4 (Rocher-Ros et al., 2023). The instrument was installed in the Faculty of Environmental Sciences and Engineering building of the Babeş-Bolyai University (46° 46′ 06.92″N, 23° 33′ 03.98″E) from 19 January 2023 till 18 September 2023. To the east of the sampling location (0–180°) is the urban city center of Cluj-Napoca adjacent to several parks with lakes, the airport, the river, a solid waste dump, and a wastewater treatment plant (WWTP).

The university building is situated in a residential area. On the opposite side, several blocks of flats, ranging from 15 to 35 m in height, have boiler vents. Approximately 120 m northeast of the inlet is the district gas boiler, which can emit CH_4 and potentially interfere with the city-wide emission investigation. The university's boiler vent is located on the far side of the building and is therefore unlikely to significantly affect the measurements.

2.2. Continuous Isotopic Measurements

The CH_4 mole fraction and isotopic composition ($\delta^{13}C$ and δ^2H) were measured using a custom-made extraction unit, coupled to an isotope ratio mass spectrometer (IRMS) operating in continuous flow mode (CH_4 system) (Röckmann et al., 2016). The isotope and mole fraction measurements were performed with an IRMS system. Although the logistical effort to deploy this system is considerable, it provides both $\delta^{13}C$ and δ^2H data with high precision.

Air was drawn via a 1/2 inch LDPE tubing attached to a pole on the side of the building 12 m above ground to the instrument at a flow rate of 16 L/min provided by a Varian scroll pump. The transfer time from the inlet to the

VAN ES ET AL. 3 of 21

Although precise temperature control of the system separates most interfering compounds, some require additional separation steps. The δ^{13} C measurements require CH₄ to be separated from CO₂ and Krypton (Schmitt et al. (2013)). The CO₂ largely remains on the preconcentration trap. After purification, CH₄ is combusted at 1150°C to CO₂, using oxygen provided by a nickel oxide wire. The CO₂ produced from CH₄ is separated from interfering amounts of Krypton by a PoraPLOTQ column (10m, \emptyset 0.32 mm) cooled to 21°C below room temperature. For δ^2 H measurements, the H₂ that is produced from CH₄ by pyrolysis at 1300°C is separated from water by a CarboPlot column (2m, \emptyset 0.32 mm) at ambient temperature. The sample was then introduced into the IRMS via the open split of a Thermo Fisher ConFlo IV device.

An isotope ratio mass spectrometer (IRMS, Delta V, Thermo Fisher) measured the isotopic composition of the CO_2 and H_2 from CH_4 . To generate a continuous time series for each isotope signature, the IRMS alternated between the CO_2 and H_2 measurements. The switch of the measurement configuration after each measurement means that the magnetic field is set to the value needed for the respective analyte gas, a peak-centering routine is executed to make sure that the collector configuration is set up correctly, and the source tuning parameters associated with the respective measurement configuration are updated. As each air aliquot is sampled separately, the air aliquots are unique for the $\delta^{13}C$ and δ^2H measurements.

The system regularly analyzed air from two cylinders with known, ambient CH_4 mole fractions and isotopic compositions. A working standard (CH_4 : 2032.0 ppb, $\delta^{13}C = -48.30 \pm 0.1\%$ and $\delta^2H = -92.07 \pm 2\%$) is used to correct for instrument drift and a target gas (CH_4 : 2487.0 ppb, $\delta^{13}C = -50.27\%$ and $\delta^2H = -130.60\%$) is used to verify instrument stability. Both the working standard and the target gas, were calibrated at Utrecht University. The working standard was calibrated against reference gasses provided by the Max Planck Institute for Biogeochemistry in Jena, Germany and the target gas against firn air samples that have been kept at Utrecht University >20 years to safeguard long-term stability (Brass & Röckmann, 2010). The system measured the working standard after four sample measurements and the target gas every six working standards. The exact sequence varied due to system errors and restarts, but to ensure good quality data, only air measurements bracketed by working standards were retained for data analysis.

Calibrated values for CH₄ mole fraction and δ values were derived from the raw values provided by the IRMS system (peak area and the isotopic composition vs. pure running gasses CO₂ and H₂, respectively) via Equations 1 and 2. Equation 1 established the CH₄ mole fraction (mf) in the sample by scaling the chromatogram peak area (Area) of the sample to the one of the working standard (ws), taking into account the injected air volume (V). The raw δ measurements for both samples and standards are initially corrected for short-term IRMS drifts using the running gas pulses. Following this, Equation 2 converts the δ value of the sample to the international isotope scales, VSMOW for δ^2 H and VPDB for δ^{13} C.

$$mf_{sample} = mf_{ws} \cdot \frac{Area_{sample}}{Area_{ws}} \cdot \frac{V_{ws}}{V_{sample}}$$
 (1)

$$\delta_{\text{sample}_{\text{international}}} = \delta_{\text{sample}_{\text{IRMS}}} + \delta_{\text{ws}_{\text{IRMS}}} + (\delta_{\text{sample}_{\text{IRMS}}} * \delta_{\text{ws}_{\text{IRMS}}})$$
 (2)

2.3. Identifying CH₄ Enhancements

 CH_4 in an air sample is a combination of the large-scale background CH_4 and additions from one or multiple sources. To identify CH_4 sources using the isotopic compositions, we first identified the CH_4 mole fraction enhancement above the background. Therefore, we applied the scgl.find_peaks function with parameters (prominence: 100, relative height: 0.6, and width: 3) in Python 3.0 to the CH_4 mole fraction data. To improve the performance of this peak finder, two corrections were applied to the CH_4 mole fraction time series. First, it was

VAN ES ET AL. 4 of 21

smoothed with window-averaging (Schmid et al. (2022)) over five points. This smoothing reduced noise in the CH_4 mole fraction time series, which was introduced by combining the two measurement lines for $\delta^{13}C$ and δ^2H . Second, some short-time CH_4 enhancements (usually night peaks) occurred on top of multiday enhancements. During these multiday enhancements, the peak finder often missed the nighttime enhancements, or included parts of the multiday enhancements in the peaks. To obtain only nighttime enhancements, a background was subtracted from the smoothed measurements. This background was defined as follows: We took the 10th percentile of the measurements in a 24-hr window, and afterward, we interpolated for each measurement before subtraction. In some cases, data points were utilized by multiple identified peaks. When this happened, we cut the data at the lowest points between these peaks.

After applying all corrections, we observed several short-term (<3h) CH₄ mole fraction enhancements of at least 100 ppb, in the following referred to as spikes. These spikes were superimposed on the daily enhancements, suggesting a very local source that would bias our analysis to very local sources. To determine the impact of this source, we evaluated the time series with and without the spikes. First, we manually identified and removed the spikes. This can introduce subjective bias and may overlook smaller spikes. Therefore, we also evaluated a subset of the data excluding the wind sector from which most spikes occurred (50° – 100°).

2.3.1. Calculating Source Signatures

To identify the source of the measured CH_4 mole fraction enhancement, we used a two-component mixing model for the CH_4 mole fraction and the isotopically substituted CH_4 (Equations 3 and 4), where the indices m, bg, and s stand for measured, background, and source, respectively. Equation 4 approximates the mass balance of the single-substituted isotopologues, where the products of δ and the mole fraction are added up. These equations separate the observed quantities into a contribution from the background and sources.

$$mf_m = mf_{bg} + mf_s \tag{3}$$

$$\delta_m * m f_m = \delta_{bg} * m f_{bg} + \delta_s * m f_s \tag{4}$$

Equations 3 and 4 can be combined and rearranged to obtain a linear relation between the inverse mole fraction $\frac{1}{mf_m}$ and the measured isotopic composition (δ_m) (Equation 5). Equation 5 is of the form $y = \frac{a}{x} + b$, where b is the isotope signature of the source δ_s . Thus, when δ_m is plotted versus $\frac{1}{mf_m}$, the y-intercept of a linear fit to the data returns δ_s . This is the so-called Keeling plot approach and requires the background mole fraction and isotopic composition to be stable (Pataki et al., 2003; Keeling, 1961). This requirement is usually met in continuous measurements as measurements at a fixed site measure both elevations and background air within a short time frame.

$$\delta_m = \frac{mf_{bg}(\delta_{bg} - \delta_s)}{mf_{ms}} + \delta_s \tag{5}$$

In the Miller-Tans approach (Miller & Tans, 2003), Equations 3 and 4 are combined and rewritten differently, leading to Equation 6. This formula has the linear form of y = ax, with $y = \delta_m * mf_m - \delta_{bg} * mf_{bg}$, $x = mf_m - mf_{bg}$, and $a = \delta_s$. Thus in this approach, the slope of a linear fit to the data returns the source isotopic composition. This method can also be applied for fluctuating background when the background is explicitly included in x and y (Defratyka et al., 2023).

$$\delta_m * mf_m - \delta_{b\varrho} * mf_{b\varrho} = \delta_s * (mf_m - mf_{b\varrho})$$
(6)

To define the background component for Equations 5 and 6, we added background data points to the data set of each identified peak, before doing the source signature analysis. Specifically, we added the three nearest points before and after the peak that were not associated with any identified peak. Furthermore, we specified a minimum amount of data points for analysis to eliminate possible artificial peaks caused by background noise or system instabilities. If the enhancement contained data for both isotopes (δ^{13} C and δ^{2} H), a minimum of four data points was required. If the enhancement contained data for a single isotope signature, the peak must consist of at least six data points. In our analysis, we compare both approaches (Keeling plot and Miller-Tans method) and flag

VAN ES ET AL. 5 of 21

 Table 1

 Meteorological Parameters During the Mobile Surveys

| | Date | Weather | T (°C) | local time | Wind direction | Wind speed (m/s) | Rain (mm) | Analyzer |
|---|------------------|---------|--------|-------------|----------------|------------------|-----------|----------|
| 1 | 23-25 May 2023 | Sunny | 14–24 | 10:00-18:00 | SW | 1–3 | 6* | Aeris 1 |
| 2 | 16 October 2023 | Sunny | 10-12 | 10:00-15:00 | W | 2–3 | 0 | None |
| 3 | 16 December 2023 | Sunny | 1–3 | 10:00-14:30 | W | 1–2 | 0 | None |
| 4 | 18 January 2024 | Cloudy | 6-10 | 10:00-15:00 | ENE | 2–3 | 0.1 | None |
| 5 | 19-21 June 2024 | Sunny | 22-31 | 7:00-18:00 | NW-SW/ENE** | 1–4 | 0 | Aeris 2 |

Note. *Only on 25 May from 14:00–15:00. **Wind direction fluctuated between these wind directions. Aeris 1: MIRA Ultra Mobile. Aeris 2: MIRA PICO.

inconsistencies between the two methods. When large discrepancies occurred between them ($\delta^2 H > 10\%$, $\delta^{13}C > 2\%$), data were thoroughly checked. Generally, the differences occurred for enhancements on the edges of the set limits, containing less than six data points, or with low CH_4 mole fraction enhancements <200 ppb. These were excluded from further analysis. For the accepted peaks, the Keeling plot intercepts were used.

2.3.2. Source Partitioning

For a formal source partitioning in the footprint area of our measurement site, we used a three-end-member mixing model where a measured source signature consists of contributions from the following three end-members: biogenic sources, natural gas from the distribution network, and combustion sources. The source signatures used the values determined from the samples collected during the mobile surveys (see the following section). The source partitioning was calculated using multiple linear regression (MLR) in MATLAB R2024b with the regress function. When a calculated source signature falls outside the range connecting the end-member points, this method produces negative contributions. In such cases, these values were set to zero, and the remaining contributions were normalized. We estimated prediction uncertainty via Monte Carlo simulation (n = 100), adding Gaussian noise to δ^{13} C and δ^2 H based on the mean measurement errors. The model was applied to each perturbed data set, and the standard deviation of predictions across simulations was used to quantify uncertainty in source contributions.

2.4. Mobile Surveys

We conducted five mobile surveys to determine CH_4 sources in Cluj-Napoca (Table 1). During the initial and final surveys, we monitored the CH_4 and C_2H_6 mole fractions using real-time laser analyzers: a MIRA Ultra Mobile for the initial survey and a MIRA PICO for the final survey, both from Aeris Technologies. The analyzer was mounted in a car and analyzed air provided via a 1/8-inch Dekabon line wrapped around the right mirror and entering the car through the window. The transfer time from the inlet to the detector was approximately 9 s. When an analyzer measured a CH_4 elevation during the mobile surveys, we tried to identify the source. When areas of interest were inaccessible by our car, we continued on foot and carried the analyzer. When walking, a 1-m piece of 1/8-inch Dekabon tubing was used as an inlet to point at potential sources.

In the surveys, we targeted potential CH₄ sources, described in Table 2. This process may introduce bias in the sampling, as we selected potential locations based on their prior knowledge and the accessibility of areas. During the three surveys without a mobile analyzer, we resampled locations identified in the first survey and added new potential locations. In addition to the mobile sampling, we sampled two direct emissions sources: the natural gas distribution network at a gas network outlet connection in the university and vehicle exhaust near the exhaust pipe of two cars, a Volkswagen Amarok with a diesel engine and a Dacia Duster with a petrol engine.

During the surveys equipped with a mobile analyzer, we collected samples when the CH_4 mole fraction was more than 100 ppb above the background. This was always feasible on foot; however, while driving, we only sampled when it was safe to halt the vehicle. In addition, background air was sampled twice on each sampling day at locations where we measured low CH_4 mole fractions. During the surveys without a mobile analyzer, additional samples were collected at locations where CH_4 emissions were found earlier and at similar types of locations. The background samples were collected outside of urban areas, where no anthropogenic sources were expected. The

VAN ES ET AL. 6 of 21

Table 2Source Types Targeted During the Mobile Surveys, the Number of Samples Taken, Number of Locations, and the Expected CH₄ Production Process

| | | | Number of samples | | | | | |
|--------------|---------------------|---|-------------------|-----|----------|---------|---------|------|
| | Number of locations | Expected CH ₄ production process | Total | May | December | January | October | June |
| Car exhausts | 2 | Pyrogenic | 2 | 0 | 0 | 0 | 0 | 2 |
| Traffic | 4 | Pyrogenic | 7 | 0 | 1 | 1 | 1 | 4 |
| Lakes | 7 | Acetoclastic methanogenesis | 12 | 5 | 1 | 1 | 1 | 4 |
| Rivers | 4 | Acetoclastic methanogenesis | 11 | 1 | 2 | 2 | 2 | 4 |
| Basements | 7 | Acetoclastic methanogenesis | 11 | 1 | 1 | 1 | 1 | 7 |
| Manholes | 7 | Acetoclastic methanogenesis | 7 | 1 | 1 | 1 | 1 | 3 |
| Waste | 5 | Acetoclastic methanogenesis | 16 | 1 | 3 | 3 | 3 | 6 |
| Gas network | 2 | Hydrogenotrophic methanogenesis | 6 | 2 | 1 | 1 | 1 | 1 |
| Gas stations | 5 | Thermogenic | 9 | 0 | 1 | 1 | 1 | 6 |

samples were collected in nontransparent aluminum coated bags, either 2L SupelTM Inert Foil Gas or 3L SKC FlexFoil®. We filled the bags using a small membrane pump (PM22874-86, KNF, France). Moisture was removed using a chemical dryer (MgClO₄) before collection in the bag. We flushed the bags once with dried sample air before collection and recorded the location and sampling time.

The air samples were analyzed at Utrecht University for CH₄ mole fraction using a model G2301 cavity ringdown greenhouse gas analyzer (Picarro, Inc.). Afterward, the CH₄ isotopic composition was determined using the IRMS system at IMAU, which is similar to the IRMS system described in Section 2.2 (Röckmann et al., 2016). At the time of the measurements, the laboratory IRMS system showed a significant mole fraction dependency. Therefore, we attempted to inject roughly similar amounts of CH_4 for all samples into the system, as follows: Samples with CH₄ < 3 ppm were measured with the standard procedure. For samples with a CH₄ mole fraction between 3 and 10 ppm, the sample admission volume was reduced to trap less CH₄ and match the peak area in the instrument with the ones of the lower mole fraction samples. Samples with a CH₄ mole fraction >10 ppm were diluted offline with high purity N2 to 2 ppm before measurement. Furthermore, the calibration strategy was different from the system used for the continuous measurements. The collected samples were measured twice for each isotope signature and the working standard three times before and after samples. Samples were corrected using the average of these six working standards. The standard error of the measurements was calculated from the sample replicates. Except for samples collected from car exhaust, we assumed that the samples contained background air and calculated the source signatures via the keeling plot approach. The keeling plot approach was applied to each location, with two to six samples per location, depending on how often the site was visited. We rejected samples that did not exceed the average background mole fraction by at least 100 ppb.

We sampled air at two WWTPs, a solid waste disposal site, and sewerages. We also sampled seven lakes and four locations along the Someşul Mic River. Additionally, we collected seven unique samples from manholes in the city center. We identified several basements that, being partially underground, often are cold and moist, causing potential for microbial production. Lastly, we sampled air near five gas stations.

2.5. Meteorological Data

Wind direction and wind speed are important for the interpretation of our data as these determine the origin of the air reaching the sampling location. Since the measurement site had no meteorological station, we used data from a measurement station 2 km northwest of the continuous measurement site (46° 46′59.9″N 23° 34′00.1″E). These were obtained from meteostat.net incorporated in the Python package meteostat. This station recorded hourly parameters, of which we used wind speed (wspd) and wind direction (wdir) to characterize the air masses reaching the measurement location. To determine the origin of CH₄ during a period with elevated mole fractions, we averaged the meteorological parameters during the top 50% of a peak.

VAN ES ET AL. 7 of 21

 Table 3

 Source Signatures Assigned to the Source Categories of the Model

| | δ^{13} C‰ | δ^2 H‰ | Reference |
|-------------|------------------|---------------|--|
| Energy | -42.0 | -175 | Menoud et al. (2022a, 2022b) |
| Residential | -32.0 | -175 | Menoud et al. (2022a, 2022b) |
| Industrial | -42.0 | -175 | Assumed to be similar to energy |
| Gas network | -64.0 | -180 | Röckmann et al. (2025) |
| Transport | -20.0 | -175 | Menoud et al. (2022a, 2022b) |
| Waste | -54.0 | -293 | Average Romania Menoud et al. (2022a, 2022b) |
| Agriculture | -64.0 | -319 | Average Europe Menoud et al. (2022a, 2022b) |
| Background | -48.3 | -89 | Continuous measurements* |

Note. Most source signatures are similar to Röckmann et al. (2016). However, note that the value for industrial emissions was reported incorrectly Röckmann et al. (2016), and the correct value is used here. *Mean of the continuous measurements data points that were within 10 ppb of the established background.

2.6. Romanian Oil and Gas

The central part of the Transylvanian Depression encompasses an important gas producing region, subcircular in shape, with a diameter of 100–120 km. Cluj-Napoca is located approximately 40 km from the western edge of the gas-bearing area. A large measurement campaign was carried out in 2020 in this region as part of the ROMEO project (Stavropoulou et al., 2023), and widespread emissions of CH₄ from the gas production infrastructure were found in Korbeń et al. (2022). These emissions may affect CH₄ levels in Cluj-Napoca, but as they are located more than 40 km away, the CH₄ from these emissions is likely mixed into the regional background when the air masses reach the city of Cluj-Napoca and does not contribute to the CH₄ elevations detected in our continuous measurements. Nevertheless, the gas used in the city of Cluj-Napoca originates from the Transylvanian region and should be isotopically similar to the gas produced there. Therefore, we use the isotopic composition of CH₄ characterized during the ROMEO-2020 campaign as the expected value for the gas network.

2.7. Simulation of CH₄ Mole Fraction and Isotopic Composition

The FLEXPART model was used to simulate CH_4 mole fraction and the contribution from different source categories in Romania. FLEXPART is an offline Lagrangian particle dispersion model (Pisso et al., 2019). Meteorological fields to drive FLEXPART were obtained from the European Centre for Medium-range Weather Forecast (ECMWF), using their high-resolution (HRES) operational analysis and short-term forecast product. Data were available hourly at $0.1^{\circ} \times 0.1^{\circ}$ horizontal resolution for a European domain (incl. Romania) and 3 hourly at $0.5^{\circ} \times 0.5^{\circ}$ resolution for the whole globe. 20,000 Lagrangian particles (air parcels) are released in the model every hour from the measurement location and followed backward for 10 days, or until they have left the European domain (-10 to 50° E, 35 to 70° N). CH_4 sink reaction were ignored, as the influence is marginal for a 10 day trajectory. When the trajectories pass CH_4 sources based on the used inventories (see below), corresponding CH_4 emissions are added to the surface layer of the model. Due to the large number of release particles, the statistical emission footprints can be calculated. This footprint is illustrated in Figure S12 in Supporting Information S1, where areas are colored by the source-receptor relationship (SRR).

The model used emissions from the TNO, CAMS-REG inventory version 5.1 (CoCO2 update) (Kuenen et al., 2022) valid for the year 2021. The inventory provides anthropogenic emissions at high spatial resolution (6 km \times 6 km) for 11 GNFR sectors. The inventory aligns with emissions reported by European countries to UNFCCC. No natural sources were considered in the FLEXPART simulations. An earlier inventory is sufficient, as anthropogenic CH₄ emissions change slowly over time. Although 2021 saw COVID-19 restrictions that may have affected emissions from traffic and industry, these are minor sources. Thus, the 2021 inventory remains suitable for the 2022/2023 study period.

In addition to providing total mole fractions, synthetic isotope time series are generated by multiplying the fractions originating from the different source sectors by their typical isotope source signatures (Table 3). The model-generated time series for CH_4 mole fraction and isotopic composition were compared to the measured time

VAN ES ET AL. 8 of 21

21698996, 2025, 18, Downloaded from https://agupubs.onlinelibrary.wiley.com/doi/10.1029/2024ID043015 by Physikalisch Tec Bundesanstalt, Wiley Online Library on [27/11/2025], See the Term

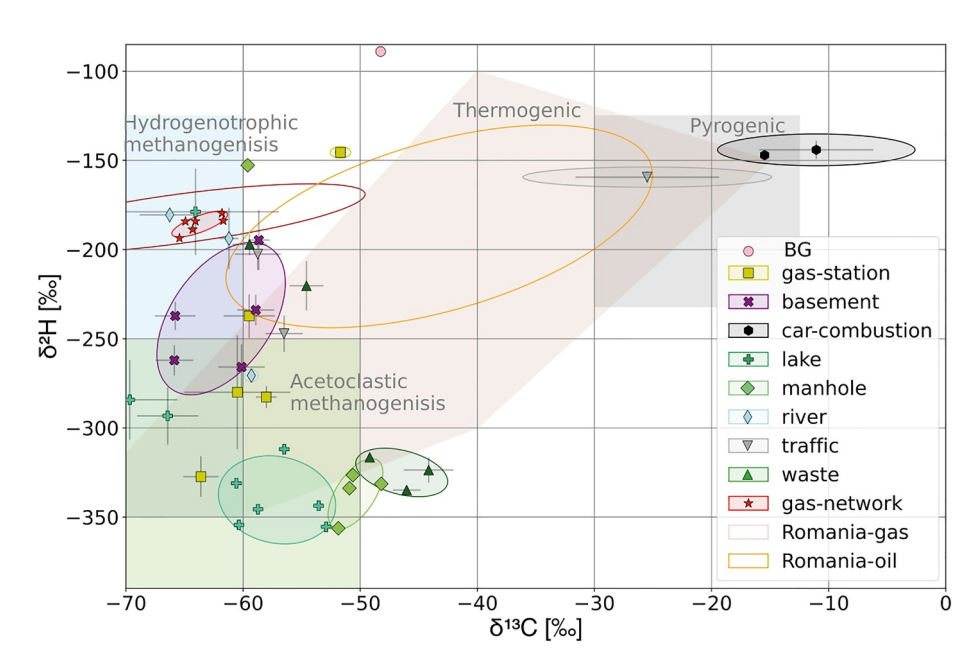


Figure 2. Dual isotope plot showing the source signatures determined from the samples collected during the mobile surveys in Cluj-Napoca. The points were fit in an ellipse with 95% certainty for different source types and are shown as color-filled ellipses. The open ellipses Romania oil and Romania gas show the range of source signatures of samples from gas production infrastructure in Transylvania and oil measurements in Romania (Menoud, Van Der Veen, Maazallahi, et al., 2022). Shaded regions indicate typical range of signatures for different CH₄ production processes (Eyer et al., 2016; Milkov & Etiope, 2018).

series to investigate if the simulations accurately reproduce the measurements. For our study, 1 month in winter (19 January–19 February 2023) and 1 month in summer (24 August–18 September 2023) were simulated to evaluate the model performance in general. In addition to these, we performed simulations with a maximum horizontal distance of 25 km to evaluate local emissions. However, note that this may yield in inaccurate results due to the low resolution associated with the large inventory grid cell sizes.

FLEXPART simulations include recent increases in CH_4 mole fraction, resulting from emissions in the transport domain. These emissions are added to the background CH_4 mole fractions fields with the values of Table 3. In our simulations, we obtain the CH_4 concentrations at the end points of all back trajectories from the "CAMS global inversion-optimized greenhouse gas fluxes and concentrations" product (v23r1 based on surface air samples; https://atmosphere.copernicus.eu/greenhouse-gases-supplementary-products last access 2024-10-28).

3. Results and Discussion

3.1. Isotopic Source Signatures From Regional CH₄ Sources

During the mobile surveys, we collected 104 discrete samples. The nine accepted background samples had an average CH_4 mole fraction of 2030 ppb and isotopic composition of $\delta^{13}C = -48.2\%$ and $\delta^2H = -91\%$. After rejection of samples with sampling or measurement errors, the accepted samples were grouped by location. For each group, the source signature was estimated via the Keeling plot approach described above, where the background isotopic composition was added to each set. The complete set of samples resulted in 46 individual source signatures. Figure 2 shows the source signatures from these sample groups colored by the source types (legend Figure 2). A table with all source signatures is provided in the Table S1.

Hydrogenotrophic methanogenesis: The samples from the gas leak and the gas network showed a similar isotopic signature. Samples from the gas network were stable throughout all seasons, indicating no change in the gas source. The CH_4 isotopic composition from the gas network is $\delta^{13}C\approx-60\%$ and $\delta^2H\approx-200\%$. This isotopic composition is typical for CH_4 produced by hydrogenotrophic methanogenesis (Whiticar, 2020). The gas used in Cluj-Napoca likely originates from the Transylvanian gas production area and is similar in isotopic composition to the gas produced there (Menoud, Veen, et al., 2022; Röckmann et al., 2025).

VAN ES ET AL. 9 of 21

Pyrogenic: Several samples targeting traffic emissions contained CH_4 at mole fractions close to background levels, due to the variation in traffic and the generally low CH_4 emissions from traffic (Popa et al., 2014). In addition, these roads were in the city center, leading to possible contamination with other sources and preluding reliable characterization of the source signature. The samples collected near the exhaust of stationary running vehicles were all elevated in the CH_4 mole fraction. The source signatures of samples from traffic and combustion with $CH_4 > 2200$ ppb were enriched in both 2H and ^{13}C , which is typical for samples that can be attributed to fossil fuel burning (Menoud, Van Der Veen, Lowry, et al., 2022). The samples below 2200 ppb were likely mixed with nearby sources as they were depleted in ^{13}C . They were sampled in the city center with many proximate sources, and they are therefore not considered in the further evaluation.

Acetoclastic methanogenesis: The CH_4 isotopic source signatures at the WWTP and sewerage were depleted in 2H , but with $\delta^{13}C$ values > -50% they are relatively enriched in ^{13}C compared to waste samples from the global database (Menoud, Van Der Veen, Lowry, et al., 2022; Sherwood et al., 2021). Sherwood et al. (2021) has nonfossil CH_4 entries only for Germany and Italy, while Menoud, Van Der Veen, Lowry, et al. (2022) also includes and Romanian wastewater samples with $\delta^{13}C$ -49.2% and $\delta^2H = -328\%$. The high $\delta^{13}C$ value could indicate a high degree of oxidation, but the low δ^2H value does not support this. The solid waste site and the field near the WWTP had lower CH_4 mole fractions (max $CH_4 = 2314$ ppb and $CH_4 = 2317$ ppb) and isotopic source signatures similar to the gas network, indicating contamination from the gas network. In the further context of this paper, we will refer to pyrogenic to be both emissions from biomass/wood burning and vehicles, as these are isotopically similar.

The isotopic source signature of the CH_4 from most lake samples indicated CH_4 production via microbial fermentation in the water. The isotopic composition is 8%e more enriched in ^{13}C than literature data; however, this offset is small (Menoud, Van Der Veen, Lowry, et al., 2022). The sample collected at Lake A, with a high CH_4 mole fraction of 3075 ppb, was likely contaminated by nearby gas leaks in the city center, as indicated by its elevated δ^2H value. The river samples at River A had a CH_4 isotopic composition similar to the lakes (Figure 1). However, the samples from River B and River C had an isotopic composition similar to the gas network, indicating possible contamination. Sample River A did not experience contamination, probably because we sampled more closely to the river bank. The highest CH_4 mole fraction at River C was recorded during ENE wind, while all others were taken during western wind. As the samples were taken north of the river, this sample is likely contaminated with other sources.

More microbial CH₄ was detected from the numerous manholes surveyed in the city center. Five of the seven samples had elevated CH₄ mole fractions. The isotopic signatures point to CH₄ production through microbial fermentation, which aligns with the wet conditions that foster an environment supporting microbial activity.

Basements: The CH₄ mole fractions in the basements were at maximum 2425 ppb and had high variability in the source signature. These source signatures were isotopically widely spread between the gas network and the microbial sources. Given that all sampled basements were located in the city center, we expected to detect CH₄ leakages from the gas distribution network. However, the consistent isotopic compositions observed across six different basements strongly suggest that the CH₄ is primarily the result of microbial processes occurring within the basements themselves, rather than an external source mixture.

Thermogenic: One of the five gas stations (gas station E) had a maximum mole fraction of 4,000 ppb with the isotopic composition $\delta^{13}C=-50.9\%e$, $\delta^2H=-142\%e$. This isotopic composition indicates thermogenic CH_4 that evaporated from fuel. The samples collected at the other gas stations have low CH_4 mole fractions between 2066 and 2225 ppb. In addition, these gas stations are near a WWTP or a lake, increasing the likelihood of contamination with nearby sources. The isotopic composition supports contamination with microbial fermentation sources. While the $\delta^{13}C$ values are comparable across all gas stations, the δ^2H values for the gas stations A–D are lower than the expected values.

3.2. Time Series

The time series for the CH₄ mole fraction, $\delta^2 H$ and $\delta^{13} C$ (Figure 3), follow a consistent pattern. An increase in CH₄ is associated with low $\delta^2 H$ and $\delta^{13} C$ values. From the time series, we defined a background component as the 10^{th} percentile of the data series. Using this definition, the background mole fraction was 2026 ppb and the background isotopic composition was $\delta^{13} C = -48.3 \pm 0.2\%$ and $\delta^2 H = -89 \pm 2.0\%$. The background CH₄

VAN ES ET AL. 10 of 21

21698996, 2025, 18, Downloaded from https://agupubs.onlinelibrary.wiley.com/doi/10.1029/2024ID043015 by Physikalisch Tee Bundesanstalt, Wiley Online Library on [27/1/2025]. See the Term

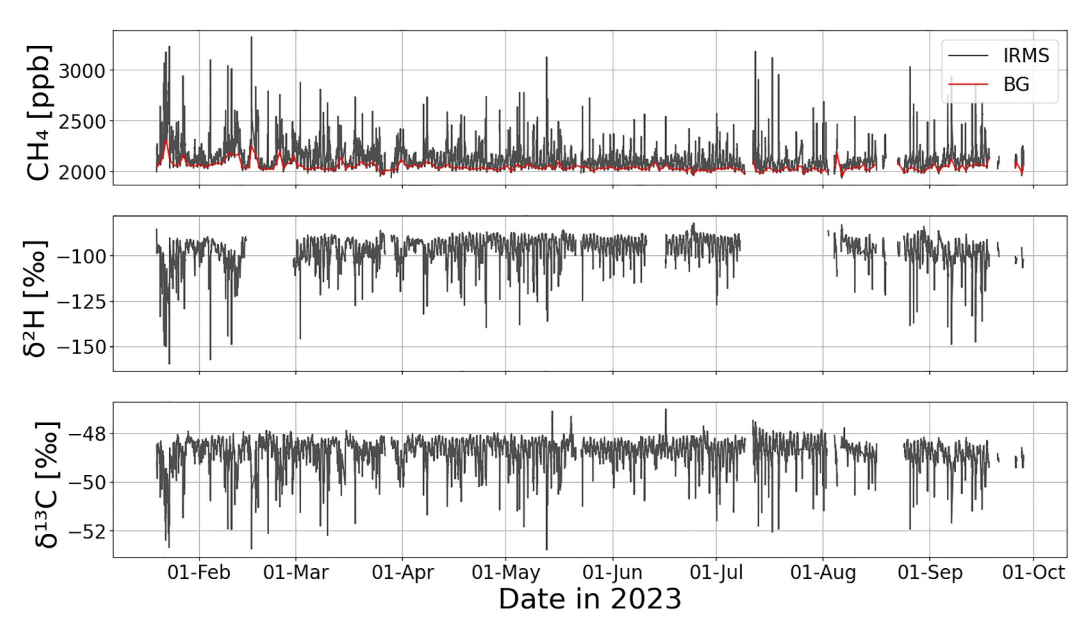


Figure 3. Time series of the continuous measurements of the CH₄ mole fraction, δ^2 H, and δ^{13} C in Cluj-Napoca from 19 January till 30 September 2023. Gaps in the time series reflect malfunctioning or servicing of the system.

isotopic values showed no variation between winter and summer. The maximum recorded CH_4 was 3234 ppb, the CH_4 amplitude (peak-to-baseline) was on average 346 ppb, and the median was 305 ppb.

Drifts in the raw data produced by the analytical system over the 9-month deployment period were corrected for using the reference gas. The accuracy is demonstrated by the difference from the assigned value (Δ). The δ^{13} C was Δ 0.004% with σ 0.15%. The δ^{2} H value was Δ 0.3% with σ 0.7%. The uncertainty for the CH₄ mole fraction of the target gas was Δ 6 ppb, and the reproducibility was \pm 46 ppb. This is rather high due to the sparsity and the system's worsening performance with higher mole fractions.

The $\mathrm{CH_4}$ background mole fraction in Cluj -Napoca is higher than similar measurements at other European locations. We compared our data to near surface data (inlet height <10m) from seven stations of the Integrated Carbon Observation System (ICOS) in Europe, with station codes PRS, PUY, BIR, TOH, OPE, LIN, and KRE, (Apadula et al., 2024; Colomb et al., 2024; Kubistin et al., 2024a; Kubistin et al., 2024b; Lund Myhre et al., 2024; Marek et al., 2024; Ramonet et al., 2024) during our measurement period. The $\mathrm{CH_4}$ background levels at the ICOS stations were 8–72 ppb lower than in Cluj -Napoca, which is larger than our measurement error of 6.1 ppb.

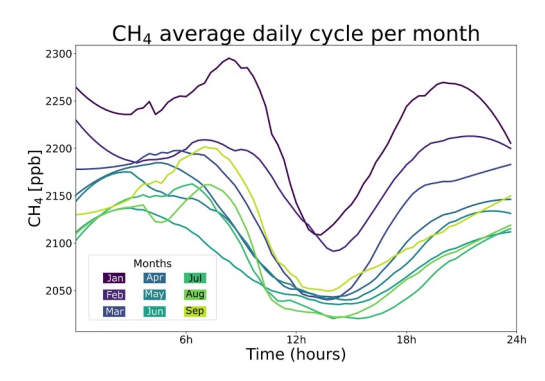


Figure 4. Average diurnal CH₄ mole fraction cycle for each month of the continuous measurement campaign. After splitting the data by month, the values were averaged over 10-min intervals and smoothed using a 30-point moving average. Time is reported in UTC, and CH₄ is expressed in ppb.

A clear diurnal cycle is observed with regular CH₄ elevations at night (Figure 4). This diurnal cycle is the dominant feature in the time series (Figure 3). CH₄ mole fractions typically returned to background values during daytime when the boundary layer is deep and turbulent conditions reduce vertical gradients. Figure 4 shows the monthly average diurnal cycles. The diurnal cycle was lower in summer (green lines) than in winter (purple lines) with the highest values in January, which is expected due to the lower and more stable nocturnal boundary layers in winter than summer. During two periods (20–23 January and 11–13 February) multiday pollution events occurred in addition to the diurnal cycle.

Occasionally, the maxima of the diurnal cycle showed an additional sharp spike, mainly toward the end of the diurnal enhancement. An example is shown in Figure 5, showing spikes on 26, 27, and 28 August. Manual identification of these spikes revealed that they regularly occurred between 6:30 and 9:00 UTC and were associated with wind directions ranging from 50° to 100° and were not related to wind speed. The observed spikes are potentially

VAN ES ET AL. 11 of 21

/doi/10.1029/2024JD043015 by Physikalisch Tec Bundesanstalt, Wiley Online Library on [27/11/2025]. See

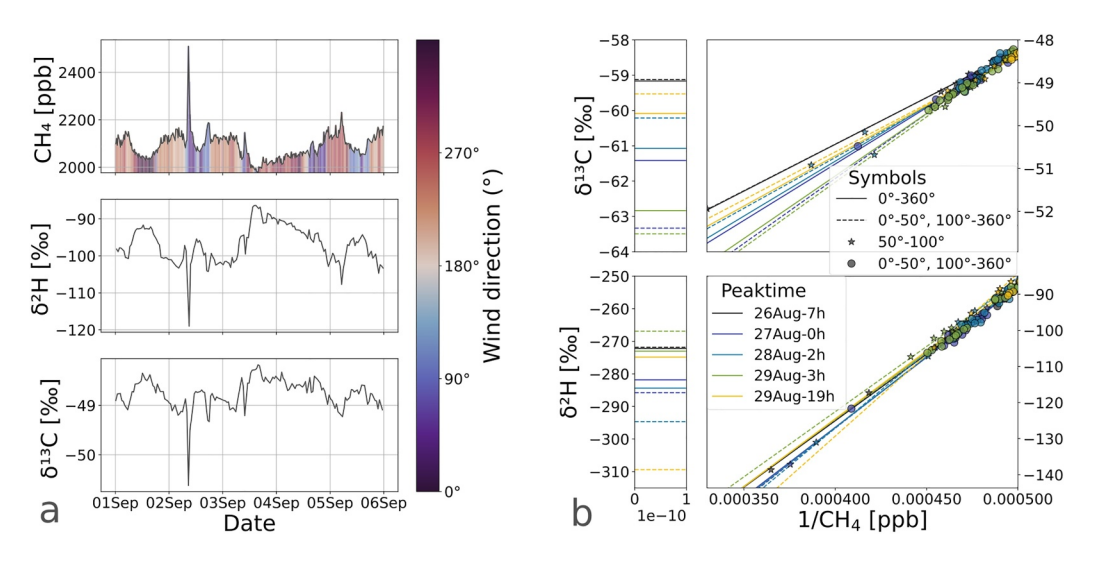


Figure 5. (a) Subset of the time series from 25 August to 30 August. The bars below the CH_4 mole fraction data curve are colored by the wind direction. (b) Keeling plot for the enhancements in (a). The stars show measurements for wind direction $50^{\circ}-100^{\circ}$, and the dots show all other wind directions. The lines are fits through the samples, with either all samples (solid) or with the wind sector excluded (dashed). The colors indicate unique dates, see legend.

 CH_4 emissions from a nearby chimney. A small chimney is located 30 m northwest of the inlet, and a larger chimney is situated 115 m to the northwest (46° 46′08.8″N, 23° 33′05.9″E).

The presence of spikes in the data set may affect the outcomes of Keeling plot analysis, as data points of the highest and lowest mole fractions predominantly influence the results. The Keeling plots corresponding to the peaks identified in Figure 5a are shown in Figure 5b. Visually, there is no clear or systematic difference between the data from the wind sector $50^{\circ}-100^{\circ}$ (stars) and the other wind directions (dots). There is also no clear difference between the bulk of the data at lower mole fractions (right side of the Keeling plot) and the few data points representing the spikes. The different lines are fits to the samples from the individual days, either including all samples (solid lines) or excluding the wind sector $50^{\circ}-100^{\circ}$ (dashed lines). This analysis reveals that omitting data from 50° to 100° only slightly affects the δ^{13} C source signatures derived from the Keeling plot, whereas the δ^{2} H source signatures shifted by between 5% and 30%. These shifts occur in both positive and negative directions and thus likely reflect variability and no systematic bias from the spikes.

3.3. Source Signatures Determined From the Continuous Measurements

The peak identification method detected 249 peaks in the CH₄ mole fraction time series, with 65 peaks lacking $\delta^2 H$ data due to system errors. Figure 6 displays the source signatures of the CH₄ enhancements with both source signatures, obtained by the keeling plot approach. A comparison between the Keeling plot and Miller-Tans source signatures can be found in the Table S1. The derived source signatures fall between -69% and -47% for $\delta^{13}C$ and -181% and -302% for $\delta^{2}H$, with the exception of two points. Most source signatures (80%) fall in an even smaller range of -55% and -65% for $\delta^{13}C$ and between -200% and -300% for $\delta^{2}H$.

The comparison of the source signatures determined from the stationary measurements and from the mobile surveys indicates that the observed enhancements in the time series are likely due to mixtures of CH_4 from gas leaks, microbial sources, and a source high in $\delta^{13}C$. Measurements at fixed locations are susceptible to source mixing, which occurs when multiple sources are located in the same wind direction relative to the measurement site. In our data set, we can identify two main types of potential source mixing. The blue shading in Figure 6 indicates mixing between CH_4 from the microbial fermentation sources and the gas network. Most of the measurements can be explained by mixing of these two source types. However, some of the high $\delta^{13}C$ values can only be explained by mixing with a third source type, enriched in $\delta^{13}C$ (red shading), which means that in Cluj, we observe a complex mix of at least three source types. The CH_4 enriched in $\delta^{13}C$ could originate from gas stations (Baciu et al., 2018; Menoud, Van Der Veen, Maazallahi, et al., 2022; Popita et al., 2015), but these emissions are generally low and the CH_4 from the gas station we measured was not sufficiently ^{13}C -enriched to explain the

VAN ES ET AL. 12 of 21

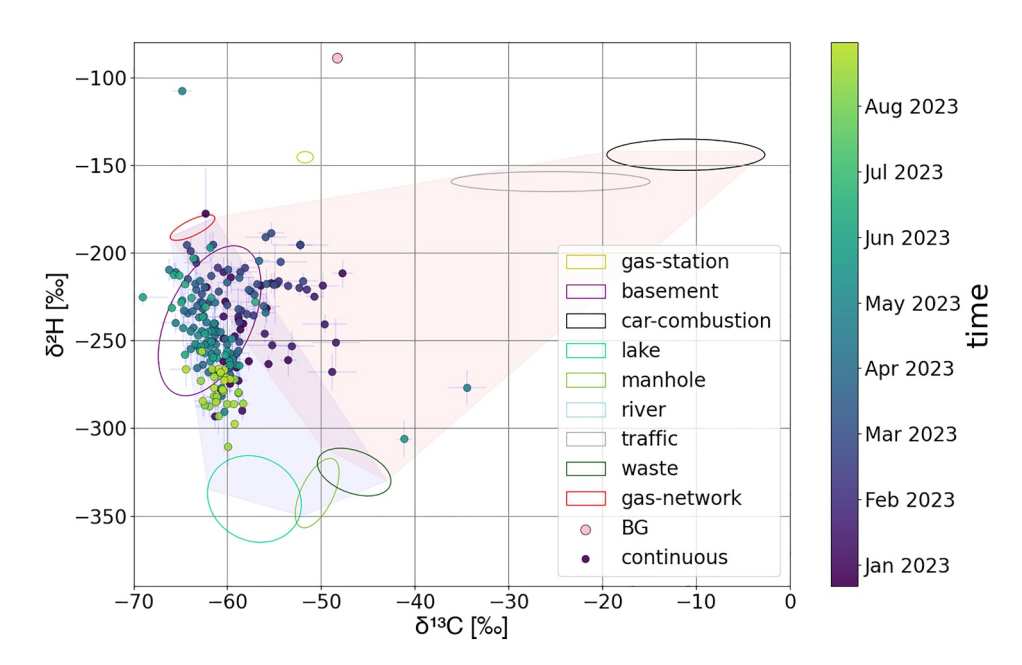


Figure 6. Dual isotope plot with CH_4 source signatures determined from the continuous measurements. Points are colored by measurement date. The open ellipses represent the distribution of samples for each source category, as determined from the mobile survey (Figure 2). The shaded blue region illustrates possible isotopic mixing between CH_4 from the gas network and the biogenic sources, and the red shading shows the mixing of these two-component mixtures and an additional source enriched in ^{13}C and ^{2}H , probably a combustion source. An alternative version where the spikes are removed and data associated with wind directions $50^{\circ}-100^{\circ}$ removed are shown in Table S1.

observed source signatures. Another potential origin could be the CH_4 from the ^{13}C -enriched waste, but this could not explain the high δ^2H values. Therefore, this source is most likely a pyrogenic source such as wood burning or traffic combustion. The samples taken near the gas exhaust of cars do agree isotopically with this pyrogenic source. These sources were not observed during the mobile measurements; however, no campaigns with mobile detectors were performed during winter. It is also possible that pyrogenic emissions originate from gas boilers in the city (Zhang et al., 2023). These emissions might be hard to detect in mobile measurements as these boilers only vent for short periods and possibly from chimneys, which may be missed by the street level surveys.

When data points associated with wind directions between 50° and 100° were removed, 197 peaks were identified. The source signatures of this subset of data exhibited a similar spread in isotopic composition as the complete data set, even though the data points spread out slightly more (Table S1). This is not solely due to the removal of spikes; normal peaks from this wind sector were also affected. Some nighttime elevations from these wind directions were entirely removed, while others were no longer identified as peaks due to an insufficient number of elevated data points.

With manual identification, we identified a total of 30 spikes. The dual isotope plot for the data set where the spikes are removed is shown in the Table S1. In this plot, some points are removed and some are slightly shifted compared to the complete data set. The points most frequently shift toward more negative δ^{13} C values and primarily affect the peaks in August. However, these shifts are minor. In the manual identification, we also see that the clear outlier (δ^2 H = $-109\%_0$ and δ^{13} C = $-64.8\%_0$) is removed, showing that this is a result of a local emission and not a nighttime accumulation. Overall, we conclude that removing either the spikes or the wind sector where these spikes occur does not lead to different results regarding the spread of source signatures observed during our campaign.

In previous deployments of our high precision dual isotope field system, the measurements always highlighted one dominant source type (Menoud, Van Der Veen, Maazallahi, et al., 2022; Röckmann et al., 2016). In Cluj-Napoca, we observe for the first time a continuous mixture of at least three end-members. Mobile studies of urban environments have identified various source mixes in cities, including gas leaks, biogenic sources from wastewater and water bodies, waste, and combustion (Baciu et al., 2018; Fernandez et al., 2022; Maazallahi

VAN ES ET AL. 13 of 21

://agupubs.onlinelibrary.wiley.com/doi/10.1029/2024JD043015 by Physikalisch Tec Bundes

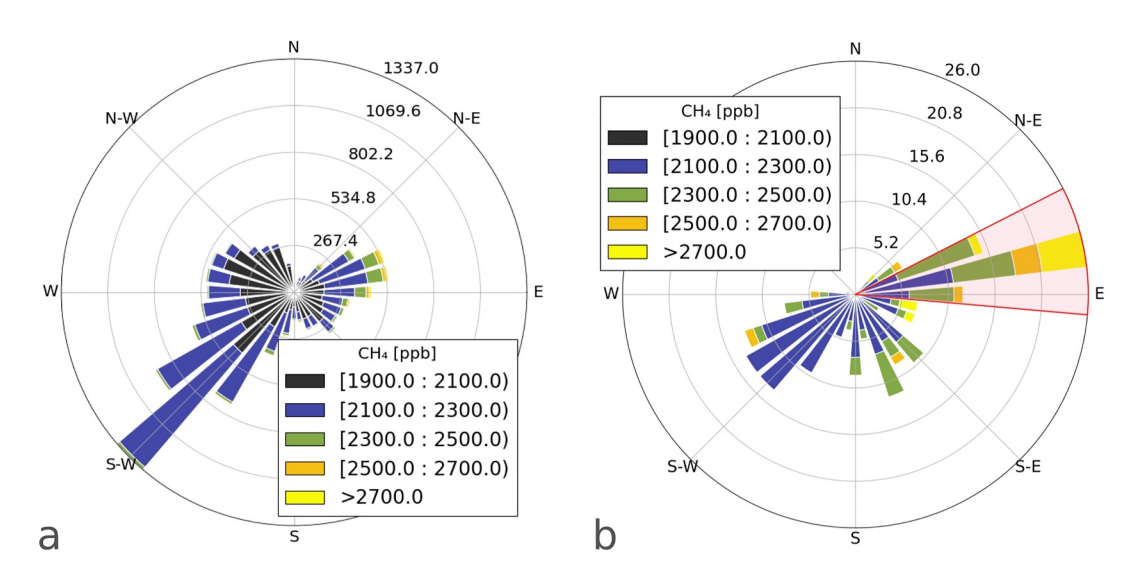


Figure 7. Wind roses binned and colored by the CH_4 mole fraction during the continuous measurements. The radial axis (raxis) represents the frequency of observations for each wind direction. (a) shows all points of the continuous measurements and (b) shows the average of the points with the 50% highest CH_4 mole fraction for each enhancement. In (b), the wind sector with the likely local source is marked in red.

et al., 2020). Our untargeted stationary measurements allow a quantitative attribution of the contributions from the different sectors.

Using a multilinear regression (Section 2.3), we established the contribution of the different end-members for each point. This is achieved by choosing three representative source categories as end-members: the gas network, the car combustion and traffic, and the four highest lake samples as these needed to be represented on the edge of the microbial. This showed contribution of $57\% \pm 4.8\%$ from the gas network, $38\% \pm 4.6\%$ biogenic contributions, and $5\% \pm 2\%$ pyrogenic sources. The winter months (January till March) had slightly higher (8%–12%) pyrogenic contributions. In summer (August and September), the emissions were mainly biogenic, 52%–60%.

3.4. Influence of Meteorological Conditions

Figure 7 shows that wind predominantly originated from the southwest and occasionally from the east and the northwest, while other wind directions were rarely observed as dictated by the orography. The wind was similar from March till September (wind roses are provided in the Table S1); the wind direction was primarily southwest and occasionally east. In these months, the highest CH₄ mole fraction originated from the east and lower mole fractions were observed from the southwest. In January and February (wind roses in the Table S1), the wind primarily came from the east and the west, respectively. However, the highest CH₄ mole fractions still came from the east, indicating that the most prominent CH₄ sources are located east of the measurement location. The meteorological parameters around the peak maxima (Figure 7) show that none of the enhancements originated from the north while the highest peaks came from the east, the location of the city center.

In Figure 8, the source signatures of the continuous measurements are colored by the wind direction. This plot shows that peaks advected from the east (city center) are generally mixtures between microbial fermentation sources and Transylvanian gas. These sources were identified during the mobile surveys (Section 3.1). The source signatures of CH_4 advected from the west are primarily a mixture of CH_4 with an isotopic composition similar to the Transylvanian gas and the ^{13}C -enriched source. No CH_4 emissions were detected on the eastern side during the mobile survey, and no nearby pyrogenic or waste sources were observed during the surveys or have been mentioned in the literature.

As mentioned in the methods and results sections, a local source is likely present in the wind direction sector 50° – 100° . These wind directions also correspond to the highest mole fractions in Figure 7. Dual isotope plots with the manually identified and removed spikes, colored by the wind direction, are shown in the Table S1. This approach only removes a fraction of the highlighted wind direction range, because excluding an entire wind sector also

VAN ES ET AL. 14 of 21

onlinelibrary.wiley.com/doi/10.1029/2024JD043015 by Physikalisch Tec Bundesanstalt, Wiley Online Library on [27/11/2025]. See the Term

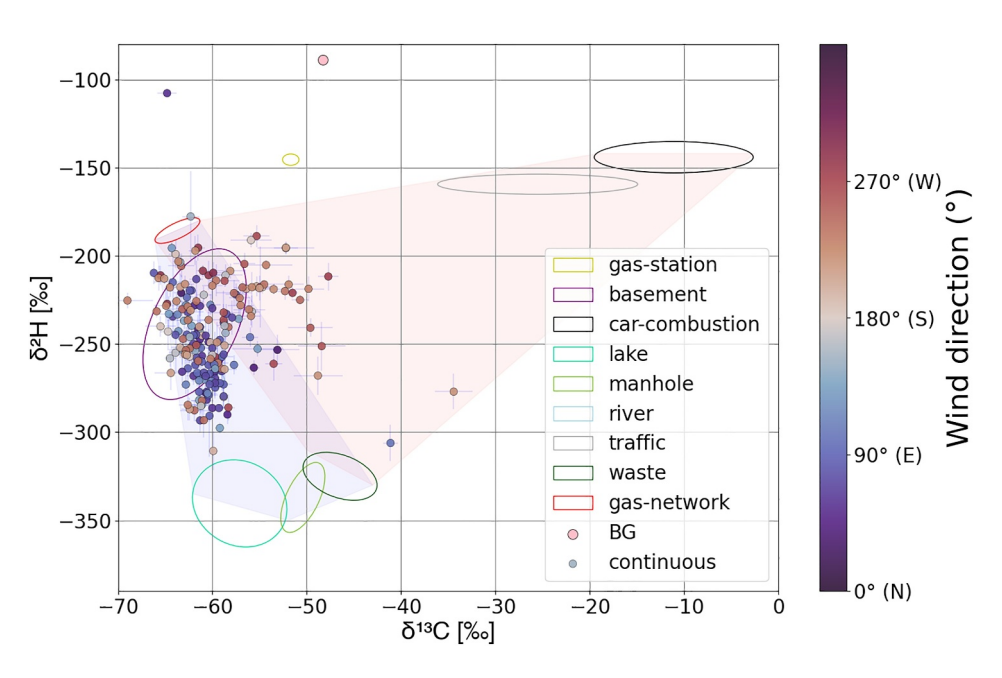


Figure 8. Dual isotope plot with CH_4 source signatures determined from the continuous measurements. Points are colored by wind direction. The open ellipses represent the distribution of samples for each source category, as determined from the mobile surveys (Figure 2). The shaded blue region illustrates possible isotopic mixing between CH_4 from the gas network and the biogenic sources, and the red shading shows the mixing of these two-component mixtures and an additional source enriched in ^{13}C and ^{2}H , which is probably a pyrogenic source.

eliminates many valid data points. The dual isotope plot with the entire wind sector removed is also shown in the Figures S2–S5 in Supporting Information S1.

Synthesizing the information from Figures 1, 6, and 8, we conclude the following. Emissions from the east (city center) represent a mix between CH_4 from the gas network and the water bodies. Waste is likely a minor source, as no large waste facilities were observed or are known on the eastern side. However, small-scale emissions such as private fermenters may still emit CH_4 . In summer, the contribution from water bodies is stronger, likely as a result of the increased microbial activity at higher temperatures. These microbial emissions could also originate from sewers as these are biogenic emissions from similar bacterial production processes (Bakkaloglu et al., 2022; Fernandez et al., 2022) found widespread sewer emissions in the city of Bucharest. The enhancements with high $\delta^{13}C$ signatures are likely pyrogenic and only occur during winter with western wind. The western side is more rural, with no obvious nonbiogenic sources. Future surveys should target these emissions; however, capturing these pyrogenic emissions accurately is difficult. They vary strongly depending on human activity and are therefore easily missed during mobile surveys. This can be addressed by sampling in tunnels, where emissions are more concentrated and less affected by other sources (Nogueira et al., 2021).

3.5. Simulated Mole Fraction and Isotopes Time Series From the Langragian Footprint

The simulated CH_4 mole, fraction and isotopic composition time series are shown in Figure 9, and the isotopes are shown in Figure S10 in Supporting Information S1. In winter, the simulated CH_4 mole fractions are consistently lower than the observations. The magnitude of the offset depends on the wind direction. Peaks advected from the west are generally predicted by the model, though the mole fraction is underestimated. The model often misses the enhancements advected from the east. Average sectorial contributions were similar in both months with the largest contributions originating from natural gas distribution and use, and waste ($\approx 35\%$ each) and agriculture ($\approx 25\%$). The simulated isotopic composition is generally more enriched for both isotopes than the measurements (Figure S10 in Supporting Information S1). This is a consequence of the mole fraction underestimation given that the sources are generally isotopically depleted compared to the background. When the mole fraction predictions are correct (Δ CH_4 < 100 ppb), the isotopic compositions are also predicted correctly (Δ $\delta^{13}C$ < 1%, Δ δ^2H < 10%) for 99% of the measurement points. The offsets for the mole fraction, $\delta^{13}C$, and δ^2H in winter were on average 120 ppb, 0.50%, and 6.6%, respectively.

VAN ES ET AL. 15 of 21

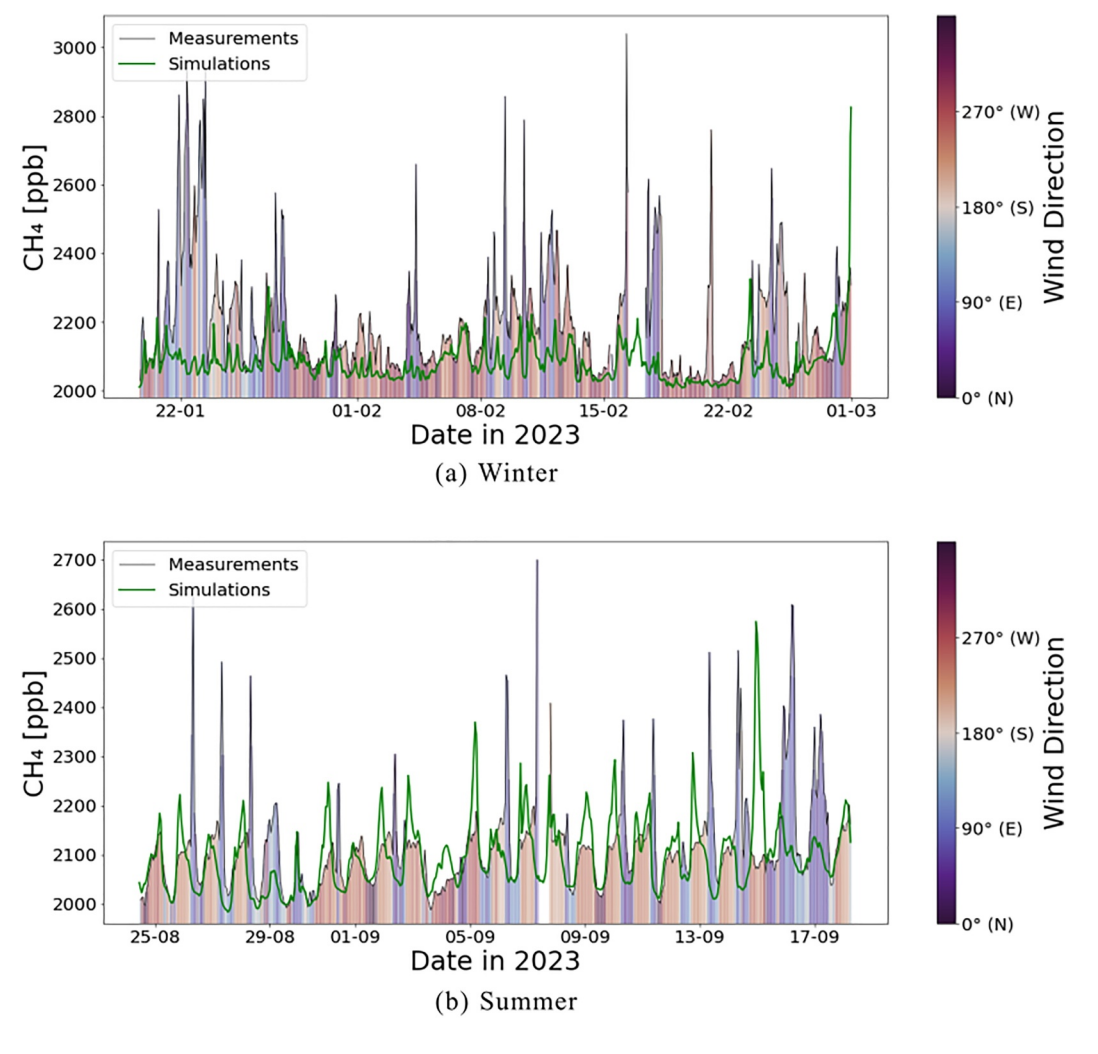


Figure 9. CH_4 mole fraction time series, both simulated (green) and measured (black) for both winter (a) and summer (b). The wind directions are shown as colored lines below CH_4 measurements. The wind direction $50^{\circ}-100^{\circ}$ is associated with spikes, which are likely very local emissions that are not present in the inventories. This figure is also available in a version with spikes filtered out in the Table S1.

The summer simulations reproduce the diurnal cycle of the CH_4 mole fraction with the typical nighttime accumulation enhancements better, but the magnitudes vary strongly. Underestimations of the simulations occur for 96% during eastern wind, while simulation overestimations occur for 100% during western wind. When CH_4 mole fraction is predicted correctly, the prediction of the isotopic composition is accurate for deuterium, but $\delta^{13}C$ values in the prediction are higher than the measurements. This could either be because the assigned source signatures are inaccurate or because the emission inventory misses CH_4 sources with depleted ^{13}C . Since the mole fraction is predicted well, it is most likely that the emission inventory considers CH_4 sources too enriched in ^{13}C . Occasionally, the model seems to predict the enhancements at the wrong time. For example, on 14 September, the model predicted a CH_4 plume during the night, while plumes with similar mole fraction occurred in the measurements the day before and after. Interestingly, the simulated enhancement differs isotopically from the neighboring measurement enhancements, suggesting that it is not simply a time shift, but a source not represented in the emission inventory and an overestimation for the predicted enhancement. The offsets for the mole fraction, $\delta^{13}C$, and δ^2H were on average 65 ppb, $0.38\%_c$, and $5.2\%_c$, respectively.

The offsets for both seasons were 93 ppb, 0.44%, and 5.9% for the mole fraction, δ^{13} C, and δ^{2} H, respectively. To evaluate the performance of the model better, we examine the source signatures. Keeling plots calculating the source signatures of the model data for both seasons are shown in Figure 10, along with the IRMS data for the

VAN ES ET AL. 16 of 21

/doi/10.1029/2024JD043015 by Physikalisch Tec Bundes

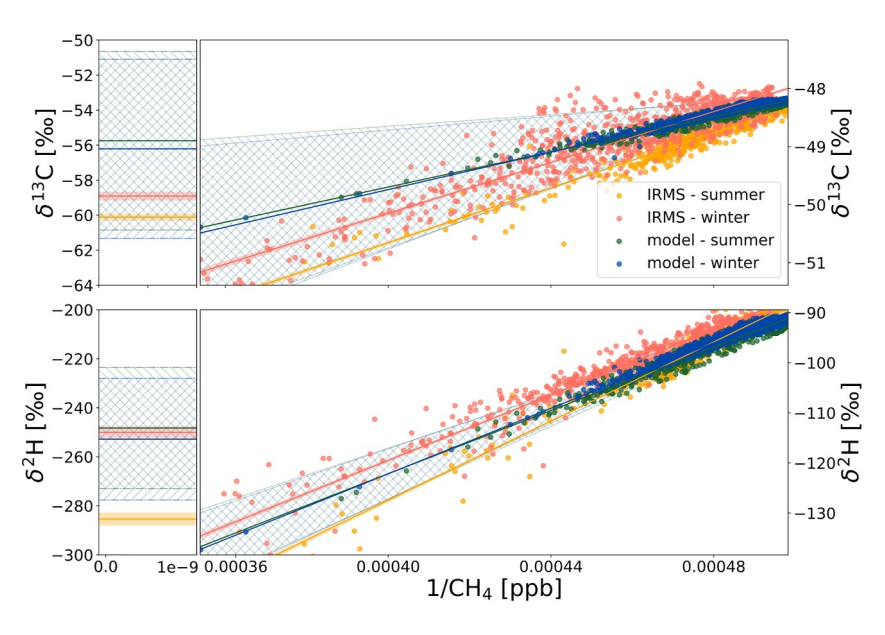


Figure 10. Keeling plot of the model data and the IRMS, for the two time periods with available simulations. The reddish colors represent the measurements, while the blueish colors represent the model.

periods when model data were available. The model consistently displays heavier source signatures than the observed data, which is either due to missing microbial sources in the inventory or an overestimation of fossil sources. Given that the modelled mole fractions are typically underestimated, a missing microbial source is most likely.

An expected reason for underestimation in the simulations is the low spatial resolution of the model and the emission inventory. The city of Cluj-Napoca is represented by only six grid cells, representing 5.56 km by 3.38 km, and the eastern side is represented by a single grid cell. This precludes a realistic representation of CH₄ transport from these sources to the measurement location in the model. The eastern side is affected to a larger degree as the enhancements occur at lower wind speeds, relating them to nearby sources.

The model did not produce the spikes that are observed in the measurement time series. This is expected since the resolution of both the model and inventory are insufficient to capture very local point sources. In both summer and winter, the model misses these spikes. During summer, when data from wind directions 50° – 100° are removed, the measurements are almost always overestimated, showing that summer model underestimations mainly come from the spikes. When the spikes were manually removed, we can still see that the model underestimates the CH₄ mole fraction from direction 50° – 100° , meaning that the model also lacks additional sources in this wind direction. No seasonality in over- or underestimation of CH₄ concentrations was observed, supporting our assumption that natural sources (lakes, rivers, and wetlands with expected larger summer emissions), although present, only minimally contributed to the observed CH₄ enhancements.

The model underestimates sources in the eastern regions, suggesting that sources are underrepresented or entirely missing in the emission inventory. The eastern wind transports Cluj-Napoca's city center emissions, with likely numerous point sources exhibiting different isotopic compositions. It is difficult to represent distributed small sources correctly in an inventory. During the mobile survey, we identified emissions from lakes, gas leaks, and waste. However, inventories show limited emissions from waste sources on the eastern side. Furthermore, the CH_4 emissions related to the public power infrastructure in the inventory are similar on the east and the west. In contrast, during our mobile surveys, these emissions were only observed within the city center, and our continuous measurements also indicate that they should be higher in the city. The model accuracy could be improved by higher resolution inventories for the city.

The regional simulations of 25 km captured most of the CH₄ peaks, showing that most emissions are very local. Maps showing these local emissions can be found in the Table S1. We observed that mainly the peaks originating from the northeast showed lower mole fractions than the simulation for the whole domain. The 25 km simulations were less influenced by biogenic sources, resulting in more enriched isotopic compositions for both δ^{13} C and δ^{2} H.

VAN ES ET AL. 17 of 21

4. Conclusions

 CH_4 mole fractions, $\delta^{13}C$, and δ^2H were measured in ambient air continuously for 9 months in Cluj-Napoca, Romania. The CH₄ mole fraction time series showed a clear diurnal cycle, with nighttime elevations generally >100 ppb, which are due to the lower and a more stable boundary layer. In addition to the nighttime elevations, we occasionally observed short spikes that likely represent local emissions. These spikes occurred between 6:30 and 9:00 and predominantly originated from wind directions between 50° and 100°.

The isotopic source signatures (δ^{13} C and δ^{2} H) calculated from the nighttime elevations show a mix of several source categories. The main source was the gas distribution network, which is similar in isotopic composition to Transylvanian natural gas. This source is rarely observed in isolation but is often mixed with biogenic fermentation sources like lakes and waste. The measurements indicate the presence of pyrogenic sources, in particular in winter. From the three end members, we estimated a total mixture of 57% gas network, 38% biogenic contributions and 5% pyrogenic. The mobile surveys revealed several CH_4 sources and highlighted the complexity of city measurements as even several point samples indicate mixtures of different sources. The gas network in Cluj-Napoca contains CH₄ produced by hydrogenotrophic methanogenesis, coming from the Transylvanian basin. The waste, manholes, and lakes all exhibited an isotopic composition indicating microbial fermentation as expected for these source types. Furthermore, we found traffic emissions with a similar isotopic composition as samples taken near car exhausts.

In the continuous measurements, we observed a variation in the isotopic composition of the CH₄ enhancements by seasons. In summer, we mainly observed a mixture between the gas network and the biogenic source, while in winter, the pyrogenic source also had a clear influence. Aside from a seasonal influence, the time series were strongly influenced by the wind direction. CH₄ elevations were only observed from the east (city center) and southwest (river valley). With eastern wind, the isotopic composition indicates a mixture between CH_4 emissions from the gas network and the microbial sources. The southwestern wind is characterized by lower CH₄ mole fractions, with isotopic compositions being a mixture between all three source categories. The pyrogenic source category was only emitted from this direction. Such a wide range of source signatures was not observed during previous continuous CH₄ isotope measurements, which were mainly dominated by one source type, with agricultural sources in the Netherlands and coal mining in Krakow (Menoud, Van Der Veen, Maazallahi, et al., 2022; Röckmann et al., 2016).

The simulations showed underestimation in winter and generally missed the peaks from the east (city center). In summer, the CH₄ simulations were overestimated during western wind but underestimated when the wind came from the city center. This is likely because the inventory does not represent the city center well, either because of missing sources or the low spatial resolution for the model and the inventory. Overall, this study shows that the inventory does not represent emissions in Cluj-Napoca well enough to allow modeling a time series on a city level. The inventory misses gas leaks on the eastern side and a pyrogenic source on the western side. Besides this, the model overestimated gas network emissions from the western side, highlighting the need for model verification with measurements.

Data Availability Statement

The continuous measurement results and the individual source signatures used in this paper are available on the ICOS Data Portal as Rockmann et al. (2024). The ICOS data used are also available on the ICOS data portal in the provided links (Apadula et al., 2024; Colomb et al., 2024; Kubistin et al., 2024a; Lund Myhre et al., 2024; Marek et al., 2024; Ramonet et al., 2024). Figures were made with Matplotlib version 3.10.0 (Team, 2024) available under the Matplotlib license at https://matplotlib.org/. Maps were created through geopandas (Bossche et al., 2024), available at https://geopandas.org/. Isotopic data from Menoud et al. (2022b), were used as isotopic value reference.

European Union's Horizon Europe Research and Innovation Programme under HORIZON-CL5-2022-D1-02 Grant Agreement No 101081430-PARIS. In addition, it is part of the project 21GRD04 isoMET project, which has received funding from the European Partnership on Metrology, cofinanced from the European Union's Horizon Europe Research and Innovation Programme and by the Participating States. Jacoline van Es was funded by Paris-horizon project.

This project has received funding from the

Acknowledgments

References

Andersen, T., Zhao, Z., de Vries, M., Necki, J., Swolkien, J., Menoud, M., et al. (2023). Local-to-regional methane emissions from the Upper Silesian Coal Basin (USCB) quantified using UAV-based atmospheric measurements. Atmospheric Chemistry and Physics, 23(9), 5191-5216. https://doi.org/10.5194/acp-23-5191-2023

Apadula, F., Heltai, D., Zazzeri, G., & Icos, R. I. (2024). ICOS atmosphere level 2 data, Plateau Rosa, release 2024-1 [Dataset]. ICOS ERIC -Carbon Portal. https://doi.org/10.18160/241A-WZ1Q

Baciu, C., Ionescu, A., & Etiope, G. (2018). Hydrocarbon seeps in Romania: Gas origin and release to the atmosphere. Marine and Petroleum Geology, 89, 130-143. https://doi.org/10.1016/j.marpetgeo.2017.06.015

VAN ES ET AL. 18 of 21



Journal of Geophysical Research: Atmospheres

- 10.1029/2024JD043015
- Bakkaloglu, S., Lowry, D., Fisher, R. E., Menoud, M., Lanoisellé, M., Chen, H., et al. (2022). Stable isotopic signatures of methane from waste sources through atmospheric measurements. *Atmospheric Environment*, 276, 119021. https://doi.org/10.1016/j.atmosenv.2022.119021
- Balcombe, P., Anderson, K., Speirs, J., Brandon, N., & Hawkes, A. (2017). The natural gas supply chain: The importance of methane and carbon dioxide emissions. ACS Sustainable Chemistry & Engineering, 5(1), 3–20. https://doi.org/10.1021/acssuschemeng.6b00144
- Basu, S., Lan, X., Dlugokencky, E., Michel, S., Schwietzke, S., Miller, J. B., et al. (2022). Estimating emissions of methane consistent with atmospheric measurements of methane and δ¹³C of methane. *Atmospheric Chemistry and Physics*, 22(23), 15351–15377. https://doi.org/10.5194/acp-22-15351-2022
- Beck, V., Chen, H., Gerbig, C., Bergamaschi, P., Bruhwiler, L., Houweling, S., et al. (2012). Methane airborne measurements and comparison to global models during BARCA. *Journal of Geophysical Research*, 117(D15), 2011JD017345. https://doi.org/10.1029/2011JD017345
- Bergamaschi, P., Segers, A., Brunner, D., Haussaire, J.-M., Henne, S., Ramonet, M., et al. (2022). High-resolution inverse modelling of European CH 4 emissions using the novel FLEXPART-COSMO TM5 4DVAR inverse modelling system. *Atmospheric Chemistry and Physics*, 22(20), 13243–13268. https://doi.org/10.5194/acp-22-13243-2022
- Bossche, J. v. d., Jordahl, K., Fleischmann, M., Richards, M., McBride, J., Wasserman, J., et al. (2024). Geopandas/geopandas: V1.0.1 [software]. https://doi.org/10.5281/zenodo.12625316
- Brass, M., & Röckmann, T. (2010). Continuous-flow isotope ratio mass spectrometry method for carbon and hydrogen isotope measurements on atmospheric methane. *Atmospheric Measurement Techniques*, 3(6), 1707–1721. https://doi.org/10.5194/amt-3-1707-2010
- Calvin, K., Dasgupta, D., Krinner, G., Mukherji, A., Thorne, P. W., Trisos, C., et al. (2023). In H. Lee, & J. Romero (Eds.), IPCC, 2023: Climate change 2023: Synthesis report. Contribution of Working Groups I, II and III to the Sixth Assessment Report of the Intergovernmental Panel on Climate Change [Core Writing Team, Tech. Rep. (1st ed.). Intergovernmental Panel on Climate Change (IPCC). https://doi.org/10.59327/IPCC/AR6-9789291691647
- Chandra, N., Patra, P. K., Fujita, R., Höglund-Isaksson, L., Umezawa, T., Goto, D., et al. (2024). Methane emissions decreased in fossil fuel exploitation and sustainably increased in microbial source sectors during 1990–2020. *Communications Earth & Environment*, 5(1), 1–15. https://doi.org/10.1038/s43247-024-01286-x
- Colomb, A., Ramonet, M., Yver-Kwok, C., Delmotte, M., Lopez, M., Pichon, J.-M., & Icos, R. I. (2024). ICOS atmosphere level 2 data [Dataset]. Puy de Dôme, release 2024-1. ICOS ERIC – Carbon Portal. https://doi.org/10.18160/HCJ9-71RG
- Defratyka, S. M., France, J. L., Fisher, R. E., Lowry, D., Fernandez, J. M., Bakkaloglu, S., et al. (2023). Statistical evaluation of methane isotopic signatures determined during near-source measurements (Preprint). *Gases/In Situ Measurement/Validation and Intercomparisons*. https://doi.org/10.5194/egusphere-2023-1490
- Defratyka, S. M., Paris, J.-D., Yver-Kwok, C., Fernandez, J. M., Korben, P., & Bousquet, P. (2021). Mapping urban methane sources in Paris, France. *Environmental Science & Technology*, 55(13), 8583–8591. https://doi.org/10.1021/acs.est.1c00859
- Dowd, E., Manning, A. J., Orth-Lashley, B., Girard, M., France, J., Fisher, R. E., et al. (2024). First validation of high-resolution satellite-derived methane emissions from an active gas leak in the UK. Atmospheric Measurement Techniques, 17(5), 1599–1615. https://doi.org/10.5194/amt-17-1599-2024
- Eyer, S., Tuzson, B., Popa, M. E., van der Veen, C., Röckmann, T., Rothe, M., et al. (2016). Real-time analysis of δ¹³C- and δD-CH₄ in ambient air with laser spectroscopy: Method development and first intercomparison results. *Atmospheric Measurement Techniques*, 9(1), 263–280. https://doi.org/10.5194/amt-9-263-2016
- Fernandez, J., Maazallahi, H., France, J., Menoud, M., Corbu, M., Ardelean, M., et al. (2022). Street-level methane emissions of Bucharest, Romania and the dominance of urban wastewater. *Atmospheric Environment: X, 13,* 100153. https://doi.org/10.1016/j.aeaoa.2022.100153
- Fiehn, A., Eckl, M., Kostinek, J., Gałkowski, M., Gerbig, C., Rothe, M., et al. (2023). Source apportionment of methane emissions from the Upper Silesian Coal Basin using isotopic signatures. *Atmospheric Chemistry and Physics*, 23(24), 15749–15765. https://doi.org/10.5194/acp-23-15749-2023
- Forstmaier, A., Chen, J., Dietrich, F., Bettinelli, J., Maazallahi, H., Schneider, C., et al. (2023). Quantification of methane emissions in Hamburg using a network of FTIR spectrometers and an inverse modeling approach. *Atmospheric Chemistry and Physics*, 23(12), 6897–6922. https://doi.org/10.5194/acp-23-6897-2023
- Hemati, M., Mahdianpari, M., Nassar, R., Shiri, H., & Mohammadimanesh, F. (2024). Urban methane emission monitoring across North America using TROPOMI data: An analytical inversion approach. *Scientific Reports*, 14(1), 9041. https://doi.org/10.1038/s41598-024-58995-8
- Henne, S., Brunner, D., Oney, B., Leuenberger, M., Eugster, W., Bamberger, I., et al. (2016). Validation of the Swiss methane emission inventory by atmospheric observations and inverse modelling. *Atmospheric Chemistry and Physics*, 16(6), 3683–3710. https://doi.org/10.5194/acp-16-3683-2016
- Hoheisel, A., & Schmidt, M. (2023). Six years of continuous carbon isotope composition measurements of methane in Heidelberg (Germany)—A study of source contributions and comparison to emission inventories (Preprint). Gases/Field Measurements/Troposphere/Physics (physical properties and processes). https://doi.org/10.5194/egusphere-2023-2079
- Hollenbeck, D., Zulevic, D., & Chen, Y. (2021). Advanced Leak detection and quantification of methane emissions using sUAS. *Drones*, 5(4), 117. https://doi.org/10.3390/drones5040117
- Hopkins, F. M., Ehleringer, J. R., Bush, S. E., Duren, R. M., Miller, C. E., Lai, C.-T., et al. (2016). Mitigation of methane emissions in cities: How new measurements and partnerships can contribute to emissions reduction strategies. *Earth's Future*, 4(9), 408–425. https://doi.org/10.1002/2016EF000381
- IEA. (2023). The imperative of cutting methane from fossil fuels.
- Keeling, C. D. (1961). The concentration and isotopic abundances of carbon dioxide in rural and marine air. *Geochimica et Cosmochimica Acta*, 24(3–4), 277–298. https://doi.org/10.1016/0016-7037(61)90023-0
- Korbeń, P., Jagoda, P., Maazallahi, H., Kammerer, J., Nęcki, J. M., Wietzel, J. B., et al. (2022). Quantification of methane emission rate from oil and gas wells in Romania using ground-based measurement techniques. *Elementa: Science of the Anthropocene*, 10(1), 00070. https://doi.org/10.1525/elementa.2022.00070
- Kubistin, D., Plaß-Dülmer, C., Arnold, S., Kneuer, T., Lindauer, M., Müller-Williams, J., et al. (2024a). ICOS atmosphere level 2 data, Lindenberg, release 2024-1 [Dataset]. ICOS ERIC Carbon Portal. https://doi.org/10.18160/3CBH-WE1Y
- Kubistin, D., Plaß-Dülmer, C., Arnold, S., Kneuer, T., Lindauer, M., Müller-Williams, J., et al. (2024b). ICOS atmosphere level 2 data, Torfhaus, release 2024-1 [Dataset]. ICOS ERIC Carbon Portal. https://doi.org/10.18160/RSY8-V8J1
- Kuenen, J., Dellaert, S., Visschedijk, A., Jalkanen, J.-P., Super, I., & Denier van der Gon, H. (2022). CAMS-REG-v4: A state-of-the-art high-resolution European emission inventory for air quality modelling. Earth System Science Data, 14(2), 491–515. https://doi.org/10.5194/essd-14-491-2022
- Lan, X., Thoning, K., & Dlugokencky, E. (2022). Trends in globally-averaged CH4, N2O, and SF6 determined from NOAA global monitoring laboratory measurements. https://doi.org/10.15138/P8XG-AA10

VAN ES ET AL. 19 of 21

- Lavoie, T. N., Shepson, P. B., Cambaliza, M. O. L., Stirm, B. H., Karion, A., Sweeney, C., et al. (2015). Aircraft-based measurements of point source methane emissions in the Barnett shale basin. *Environmental Science & Technology*, 49(13), 7904–7913. https://doi.org/10.1021/acs.est 5b00410
- Liu, M., Van Der A, R., Van Weele, M., Bryan, L., Eskes, H., Veefkind, P., et al. (2024). Current potential of CH₄ emission estimates using TROPOMI in the Middle East. Atmospheric Measurement Techniques, 17(17), 5261–5277. https://doi.org/10.5194/amt-17-5261-2024
- Lu, X., Harris, S. J., Fisher, R. E., France, J. L., Nisbet, E. G., Lowry, D., et al. (2021). Isotopic signatures of major methane sources in the coal seam gas fields and adjacent agricultural districts, Queensland, Australia. Atmospheric Chemistry and Physics, 21(13), 10527–10555. https://doi.org/10.5194/acp-21-10527-2021
- Lund Myhre, C., Platt, S. M., Lunder, C., Hermansen, O., & Icos, R. I. (2024). ICOS atmosphere level 2 data, Birkenes, release 2024-1 [Dataset]. ICOS ERIC Carbon Portal. https://doi.org/10.18160/YHQZ-3K0D
- Maazallahi, H., Fernandez, J. M., Menoud, M., Zavala-Araiza, D., Weller, Z. D., Schwietzke, S., et al. (2020). Methane mapping, emission quantification, and attribution in two European cities: Utrecht (NL) and Hamburg (DE). Atmospheric Chemistry and Physics, 20(23), 14717–14740. https://doi.org/10.5194/acp-20-14717-2020
- MacFarling Meure, C., Etheridge, D., Trudinger, C., Steele, P., Langenfelds, R., family=Ommen, p. u., et al. (2006). Law Dome CO2, CH4 and N2O ice core records extended to 2000 years BP. *Geophysical Research Letters*, 33(14). https://doi.org/10.1029/2006GL026152
- Marek, M. V., Vítková, G., Komínková, K., & Icos, R. I. (2024). ICOS Atmosphere Level 2 data, Křešín u Pacova, release 2024-1 [Dataset]. ICOS ERIC Carbon Portal. https://doi.org/10.18160/V5GW-HBT4
- Menoud, M., Van Der Veen, C., Lowry, D., Fernandez, J. M., Bakkaloglu, S., France, J. L., et al. (2022b). New contributions of measurements in Europe to the global inventory of the stable isotopic composition of methane. *Earth System Science Data*, 14(9), 4365–4386. https://doi.org/10.5194/essd-14-4365-2022
- Menoud, M., Van Der Veen, C., Lowry, D., Fernandez, J. M., Bakkaloglu, S., France, J. L., et al. (2022a). Global inventory of the stable isotopic composition of methane surface emissions, augmented by new measurements in Europe (Preprint). *Atmospheric Chemistry and Physics*. https://doi.org/10.5194/essd-2022-30
- Menoud, M., Van Der Veen, C., Maazallahi, H., Hensen, A., Velzeboer, I., Van Den Bulk, P., et al. (2022). CH4 isotopic signatures of emissions from oil and gas extraction sites in Romania. *Elementa: Science of the Anthropocene*, 10(1), 00092. https://doi.org/10.1525/elementa.2021.
- Menoud, M., Van der Veen, C., Necki, J., Bartyzel, J., Szénási, B., Stanisavljević, M., et al. (2021). Methane (ch₄) sources in Krakow, Poland: Insights from isotope analysis. *Atmospheric Chemistry and Physics*, 21(17), 13167–13185. https://doi.org/10.5194/acp-21-13167-2021
- Menoud, M., Van Der Veen, C., Scheeren, B., Chen, H., Szénási, B., Morales, R. P., et al. (2020). Characterisation of methane sources in Lutjewad, The Netherlands, using quasi-continuous isotopic composition measurements. *Tellus B: Chemical and Physical Meteorology*, 72(1), 1823733. https://doi.org/10.1080/16000889.2020.1823733
- Milkov, A. V., & Etiope, G. (2018). Revised genetic diagrams for natural gases based on a global dataset of >20,000 samples. *Organic Geochemistry*, 125, 109–120. https://doi.org/10.1016/j.orggeochem.2018.09.002
- Miller, J. B., & Tans, P. P. (2003). Calculating isotopic fractionation from atmospheric measurements at various scales. *Tellus B: Chemical and Physical Meteorology*, 55(2), 207. https://doi.org/10.3402/tellusb.v55i2.16697
- Nisbet, E. G., Manning, M. R., Dlugokencky, E. J., Michel, S. E., Lan, X., Röckmann, T., et al. (2023). Atmospheric methane: Comparison between methane's record in 2006–2022 and during glacial terminations. *Global Biogeochemical Cycles*, 37(8), e2023GB007875. https://doi.org/10.1029/2023GB007875
- Nogueira, T., Kamigauti, L. Y., Pereira, G. M., Gavidia-Calderón, M. E., Ibarra-Espinosa, S., family=Oliveira, p. u., et al. (2021). Evolution of vehicle emission factors in a megacity affected by extensive biofuel use: Results of tunnel measurements in São Paulo. *Brazil. Environmental Science & Technology*, 55(10), 6677–6687. https://doi.org/10.1021/acs.est.1c01006
- Nzotungicimpaye, C.-M., MacIsaac, A. J., & Zickfeld, K. (2023). Delaying methane mitigation increases the risk of breaching the 2°C warming limit. Communications Earth & Environment, 4(1), 1–8. https://doi.org/10.1038/s43247-023-00898-z
- Ocko, I. B., Sun, T., Shindell, D., Oppenheimer, M., Hristov, A. N., Pacala, S. W., et al. (2021). Acting rapidly to deploy readily available methane mitigation measures by sector can immediately slow global warming. *Environmental Research Letters*, 16(5), 054042. https://doi.org/10.1088/1748-9326/abf9c8
- Pataki, D. E., Ehleringer, J. R., Flanagan, L. B., Yakir, D., Bowling, D. R., Still, C. J., et al. (2003). The application and interpretation of keeling plots in terrestrial carbon cycle research. *Global Biogeochemical Cycles*, 17(1), 2001GB001850. https://doi.org/10.1029/2001GB001850
- Petrescu, A. M. R., Qiu, C., Ciais, P., Thompson, R. L., Peylin, P., McGrath, M. J., et al. (2021). The consolidated European synthesis of CH₄ and N₂ O emissions for the European union and United Kingdom: 1990–2017. *Earth System Science Data*, 13(5), 2307–2362. https://doi.org/10.5194/essd-13-2307-2021
- Pisso, I., Sollum, E., Grythe, H., Kristiansen, N. I., Cassiani, M., Eckhardt, S., et al. (2019). The Lagrangian particle dispersion model FLEXPART version 10.4. Geoscientific Model Development. 12(12), 4955–4997. https://doi.org/10.5194/gmd-12-4955-2019
- Plant, G., Kort, E. A., Murray, L. T., Maasakkers, J. D., & Aben, I. (2022). Evaluating urban methane emissions from space using TROPOMI methane and carbon monoxide observations. *Remote Sensing of Environment*, 268, 112756. https://doi.org/10.1016/j.rse.2021.112756
- Popa, M. E., Vollmer, M. K., Jordan, A., Brand, W. A., Pathirana, S. L., Rothe, M., & Röckmann, T. (2014). Vehicle emissions of greenhouse gases and related tracers from a tunnel study: CO: CO₂, N₂O: CO₂, CH₄: CO₂, O₂: CO₂ ratios, and the stable isotopes ¹³C and ¹⁸O in CO₂ and CO. Atmospheric Chemistry and Physics, 14(4), 2105–2123. https://doi.org/10.5194/acp-14-2105-2014
- Popita, G.-E., Frunzeti, N., Ionescu, A., Lazar, A.-L., Baciu, C., Popovici, A., et al. (2015). Evaluation of carbon dioxide and methane emission from Cluj-Napoca municipal landfill, Romania. *Environmental Engineering and Management Journal*, 14(6), 1389–1398. https://doi.org/10.30638/eemj.2015.151
- Ramonet, M., Conil, S., Delmotte, M., Laurent, O., Lopez, M., & Icos, R. I. (2024). ICOS Atmosphere Level 2 data, Observatoire pérenne de l'environnement, release 2024-1 [Dataset]. ICOS ERIC Carbon Portal. https://doi.org/10.18160/5QAD-ZBT3
- Ramsden, A. E., Ganesan, A. L., Western, L. M., Rigby, M., Manning, A. J., Foulds, A., et al. (2022). Quantifying fossil fuel methane emissions using observations of atmospheric ethane and an uncertain emission ratio. *Atmospheric Chemistry and Physics*, 22(6), 3911–3929. https://doi.org/10.5194/acp-22-3911-2022
- Rocher-Ros, G., Stanley, E. H., Loken, L. C., Casson, N. J., Raymond, P. A., Liu, S., et al. (2023). Global methane emissions from rivers and streams. *Nature*, 621(7979), 530–535. https://doi.org/10.1038/s41586-023-06344-6
- Röckmann, T., Eyer, S., Van Der Veen, C., Popa, M. E., Tuzson, B., Monteil, G., et al. (2016). In situ observations of the isotopic composition of methane at the Cabauwtall tower site. Atmospheric Chemistry and Physics, 16(16), 10469–10487. https://doi.org/10.5194/acp-16-10469-2016
 Röckmann, T., Menoud, M., & van Es, J. (2025). Measurement report: Isotopic composition of CH4 emitted from gas exploration sites in the

VAN ES ET AL. 20 of 21

Transvlvanian basin, Romania.

- Rockmann, T., van Es, J., & van der Veen, C. (2024). Atmospheric GHG data product (ch4, ch4_stdev, 13ch4, 13ch4_stdev, d2h_ch4, d2h_ch4_stdev) from Cluj Napoca (6.0 m) | ICOS [Dataset]. https://doi.org/10.18160/NXYQ-Y64M
- Saunois, M., Stavert, A. R., Poulter, B., Bousquet, P., Canadell, J. G., Jackson, R. B., et al. (2020). The global methane budget 2000–2017. *Earth System Science Data*, 12(3), 1561–1623. https://doi.org/10.5194/essd-12-1561-2020
- Schmid, M., Rath, D., & Diebold, U. (2022). Why and how Savitzky–Golay filters should be replaced. ACS Measurement Science Au, 2(2), 185–196. https://doi.org/10.1021/acsmeasuresciau.1c00054
- Schmitt, J., Seth, B., Bock, M., Van Der Veen, C., Möller, L., Sapart, C. J., et al. (2013). On the interference of Kr during carbon isotope analysis of methane using continuous-flow combustion–isotope ratio mass spectrometry. *Atmospheric Measurement Techniques*, 6(5), 1425–1445. https://doi.org/10.5194/amt-6-1425-2013
- Sherwood, O. A., Schwietzke, S., & Lan, X. (2021). Global δ13c-ch4 source signature inventory 2020. Earth System Research Laboratories. https://doi.org/10.15138/qn55-e011
- Stavropoulou, F., Vinković, K., Kers, B., De Vries, M., Van Heuven, S., Korbeń, P., et al. (2023). High potential for CH₄ emission mitigation from oil infrastructure in one of EU's major production regions (Preprint). Gases/Field Measurements/Troposphere/Chemistry (chemical composition and reactions). https://doi.org/10.5194/egusphere-2023-247
- Team, T. M. D. (2024). Matplotlib: Visualization with python [software]. Zenodo. https://doi.org/10.5281/zenodo.14464227
- Thanwerdas, J., Saunois, M., Berchet, A., Pison, I., & Bousquet, P. (2024). Investigation of the renewed methane growth post-2007 with high-resolution 3-D variational inverse modeling and isotopic constraints. *Atmospheric Chemistry and Physics*, 24(4), 2129–2167. https://doi.org/10.5194/acp-24-2129-2024
- Townsend-Small, A., Botner, E. C., Jimenez, K. L., Schroeder, J. R., Blake, N. J., Meinardi, S., et al. (2016). Using stable isotopes of hydrogen to quantify biogenic and thermogenic atmospheric methane sources: A case study from the Colorado Front range. *Geophysical Research Letters*, 43(21). https://doi.org/10.1002/2016GL071438
- Townsend-Small, A., Tyler, S. C., Pataki, D. E., Xu, X., & Christensen, L. E. (2012). Isotopic measurements of atmospheric methane in Los Angeles, California, USA: Influence of "fugitive" fossil fuel emissions. *Journal of Geophysical Research*, 117(D7), 2011JD016826. https://doi.org/10.1029/2011JD016826
- United Nations. (2019). World Urbanization Prospects the 2018 Revision (No. ST/ESA/SER.A/420).
- Weller, Z. D., Hamburg, S. P., & von Fischer, J. C. (2020). A national estimate of methane leakage from pipeline mains in natural gas local distribution systems. *Environmental Science & Technology*, 54(14), 8958–8967. https://doi.org/10.1021/acs.est.0c00437
- Whiticar, M. J. (2020). The biogeochemical methane cycle. In H. Wilkes (Ed.), *Hydrocarbons, Oils and Lipids: Diversity, Origin, Chemistry and Fate* (pp. 1–78). Springer International Publishing. https://doi.org/10.1007/978-3-319-54529-5_5-1
- Zavala-Araiza, D., Herndon, S. C., Roscioli, J. R., Yacovitch, T. I., Johnson, M. R., Tyner, D. R., et al. (2018). Methane emissions from oil and gas production sites in Alberta, Canada. *Elementa: Science of the Anthropocene*, 6, 27. https://doi.org/10.1525/elementa.284
- Zhang, M., Gao, L., Wang, Q., Xie, D., Gao, J., Wang, S., & Lu, X. (2023). Methane leakage measurement of natural gas heating boilers and greenhouse gas emissions accounting of "coal-to-gas" transition for residential heating in rural Beijing. *Environmental Science and Technology Letters*, 10(1), 93–97. https://doi.org/10.1021/acs.estlett.2c00751

VAN ES ET AL. 21 of 21